RSC Advances

PAPER

View Article Online
View Journal | View Issue

Cite this: *RSC Adv.*, 2025, **15**, 6634

Recycling paper sludge into hydrochar and ZnO nanocomposite for enhanced ammonium adsorption in aqueous solutions

Van Hung Hoang,[a] Thi Minh Phuong Nguyen,[bc] Thi Dong Nguyen,[d] Thi Hong Vien Nguyen,[d] Thi Hong Huyen Chu,[d] Le Phuong Hoang,[e] Phan Quang Thang,[f] Lan Huong Nguyen,[g] Trung Kien Hoang*[d] and Huu-Tap Van *[a]

This study investigates the ammonium (NH_4^+) adsorption capabilities of hydrochar derived from paper waste sludge (PWSH) and its modified variant with ZnO (PWSH@ZnO).This study investigates the ammonium (NH_4^+) adsorption capabilities of hydrochar derived from paper waste sludge (PWSH) and its modified variant with ZnO (PWSH@ZnO). The adsorption behaviors were analyzed by varying parameters such as pH, contact time, initial NH_4^+ concentration, and ZnO modification ratios. The results indicate that ZnO modification significantly enhances the NH_4^+ adsorption capacity, with PWSH@ZnO achieving a maximum capacity of 23.08 mg g^{-1}, compared to 20.09 mg g^{-1} for unmodified PWSH. The optimal pH for NH_4^+ removal was found to be 8, at which PWSH@ZnO demonstrated a superior removal efficiency of 80%, compared to 68.03% for PWSH. Kinetic studies revealed that the adsorption process followed a pseudo-first-order model for both materials, with PWSH@ZnO exhibiting faster adsorption rates. Isotherm analysis further indicated that the adsorption is best represented by the Langmuir model, suggesting monolayer adsorption on a homogeneous surface. Overall, the incorporation of ZnO nanoparticles enhanced the adsorption capacity and improved the material's stability, positioning PWSH@ZnO as a promising candidate for NH_4^+ removal in wastewater treatment applications. The synthesized PWSH@ZnO also demonstrates commendable reusability, maintaining nearly 50% of its initial adsorption capacity after five cycles.

Received 21st January 2025
Accepted 23rd February 2025

DOI: 10.1039/d5ra00493d

rsc.li/rsc-advances

Introduction

Ammonium (NH_4^+) is a prevalent nutrient in industrial, agricultural, and municipal wastewater streams. Eutrophication, a significant environmental issue, is often driven by elevated NH_4^+ concentrations in aquatic systems. This phenomenon can disrupt ecological balance and significantly degrade water quality.[1] In response to the challenge of removing NH_4^+ from wastewater, a range of technologies has been developed, including biological nitrification–denitrification, ion exchange, chemical precipitation, membrane filtration, and adsorption.[2,3] Each of these methods has distinct advantages and limitations, which must be carefully evaluated for effective implementation. Although biological processes are highly effective;[4] they require precise control of environmental conditions and are often time-consuming. Ion exchange is highly efficient but often incurs high operational costs due to the need for frequent resin regeneration.[5] While chemical precipitation effectively removes ammonium, it may introduce secondary pollutants into the system. Membrane filtration, despite its high efficiency, often faces challenges such as high energy consumption and membrane fouling.[6] Therefore, selecting an appropriate NH_4^+ removal method requires a comprehensive evaluation of both technical and economic factors to ensure sustainable wastewater treatment.

Among the various technologies available for NH_4^+ removal, adsorption stands out due to its cost-effectiveness, operational simplicity, and environmental safety.[7] This process generates

[a]*Thai Nguyen University, Tan Thinh Ward, Thai Nguyen City, Vietnam. E-mail: vanhuutap@tnu.edu.vn*

[b]*Faculty of Environmental and Natural Sciences, Duy Tan University, Da Nang 550000, Vietnam*

[c]*Institute of Research and Development, Duy Tan University, Da Nang 550000, Vietnam*

[d]*Faculty of Natural Resources and Environment, TNU – University of Sciences, Tan Thinh Ward, Thai Nguyen City, Vietnam. E-mail: kienht@tnus.edu.vn*

[e]*Faculty of Civil and Environmental Engineering, Thai Nguyen University of Technology (TNUT), Tich Luong Ward, Thai Nguyen City, Vietnam*

[f]*Institute of Science and Technology for Energy and Environment, Vietnam Academy of Science and Technology, 18 Hoang Quoc Viet Street, Cay Giay District, Ha Noi City, Vietnam*

[g]*Faculty of Biology and Environment, Ho Chi Minh City University of Industry and Trade (HUIT), 140 Le Trong Tan Street, Tay Thanh Ward, Tan Phu District, Ho Chi Minh City, Vietnam*

minimal harmful by-products and is compatible with existing wastewater treatment infrastructures, enabling seamless integration into current systems. Furthermore, a wide range of adsorbent materials, such as zeolites,[8] alumina,[9] biochar,[10,11] hydrochar,[1] chitosan porous beads reinforced with epoxy resin[12] and MOF-based modified adsorbents,[13] allows for the customization of adsorption systems to target specific contaminants, including NH_4^+. Adsorption is preferred for NH_4^+ removal due to its operational versatility across a wide range of pH and temperature conditions, minimal sludge generation, and the feasibility of adsorbent regeneration and reuse, which enhance its sustainability. Additionally, the development of cost-effective and environmentally friendly adsorbents, especially those derived from agricultural waste or natural minerals, has further enhanced the appeal of adsorption as a green wastewater treatment technology. Given these advantages, adsorption is increasingly recognized as a superior method for NH_4^+ removal from various wastewater streams, effectively balancing performance, cost, and environmental impact. These attributes make adsorption a promising and sustainable solution for NH_4^+ removal, outperforming many conventional methods in terms of efficiency, cost, and environmental compatibility.

Hydrochar, an economically viable material, is produced *via* hydrothermal carbonization of biomass at relatively low temperatures (180–350 °C) under autogenous pressure for several hours.[14] It is derived from various feedstocks, including wood, bamboo, sludge, agricultural residues, and forestry wastes. Hydrochar contains functional groups such as hydroxyl, phenolic, carbonyl, and carboxylic groups, which make it a promising adsorbent for removing contaminants, including heavy metals and organic/inorganic substances.[15] Hydrochar is also effective in removing organic dyes. For instance, alkali-modified hydrochar derived from persimmon peel showed a maximum adsorption capacity of 278.41 mg g^{-1} for methylene blue, highlighting its strong affinity for cationic dyes.[16] This affinity results from chemisorption, which is enhanced by the structural modifications of hydrochar. Hydrochar has significant environmental benefits. Its production from biomass offers a sustainable waste management solution and contributes to the circular economy by recovering valuable resources from waste materials.[17] Additionally, hydrochar's ability to remove heavy metals from aqueous solutions makes it a viable option for water purification, addressing critical environmental challenges.[18,19]

Despite its potential, hydrochar is limited by poor porosity and a small surface area. Therefore, hydrochar modifications are required to increase its surface area and porosity, enhancing its adsorption efficacy. Recent advancements include the incorporation of high-surface-area nanoparticles into activated carbon to develop efficient and cost-effective adsorbents for wastewater treatment. Among these nanomaterials, zinc oxide (ZnO) nanoparticles have been widely studied for their pollutant adsorption capabilities in aqueous environments. For instance, biochar-supported ZnO nanoparticles have been shown to remove 91% of phenol, 94% of methylene blue, and 90% of rhodamine B from water,[20] while cellulose/starch/activated carbon-ZnO (C/S/AC-ZnO) exhibited adsorption capacities of 142.70 mg g^{-1} for methylene blue and 72.63 mg g^{-1} for methyl orange 21. Additionally, Yu *et al.* (2018) found that incorporating 30% wt ZnO into biochar significantly improved chromium(VI) removal, with rates exceeding 95%.[21]

The paper industry generates significant amounts of paper waste sludge (PWS), posing substantial environmental challenges. The production rate of PWS typically ranges from 100 to 500 kg per ton of paper, depending on the factory type.[22] Traditional PWS disposal methods, including composting, incineration, and landfilling, face economic, environmental, and societal challenges.[23] Recent studies have investigated the use of recycled PWS as an adsorbent for wastewater treatment, offering significant environmental and economic benefits. For example, Ali *et al.* (2018) demonstrated that PWS effectively removed copper(II) ions from wastewater, with a maximum adsorption capacity of 114.42 mg g^{-1}.[23] Nguyen *et al.* (2021) found that $FeCl_3$-modified hydrochar derived from PWS exhibited a high capacity for NH_4^+ adsorption from aqueous solutions.[1] Despite these advancements, a notable gap remains in the literature on the incorporation of ZnO nanoparticles into PWS-derived hydrochar for NH_4^+ removal from aqueous solutions. The integration of ZnO nanoparticles is promising due to their high surface area and enhanced adsorption capabilities, as demonstrated in previous studies.[24,25] Developing such hybrid materials could significantly enhance NH_4^+ removal efficiency, contributing to more sustainable wastewater treatment solutions.

This study introduces a novel adsorbent by modifying PWS-derived hydrochar with ZnO nanoparticles (ZnO-NPs) for NH_4^+ removal from wastewater. While hydrochar and biochar have been widely studied as adsorbents, the application of ZnO-modified PWS-derived hydrochar for NH_4^+ removal remains underexplored. This research addresses key environmental challenges, such as PWS disposal and water resource contamination, while offering a low-cost, efficient adsorbent with enhanced surface area and adsorption properties. The combination of ZnO nanoparticles with hydrochar aims to enhance surface reactivity and overcome the limitations of traditional hydrochar, such as low porosity and limited surface area. This innovative approach represents a pioneering effort to develop cost-effective, eco-friendly materials for NH_4^+ removal, contributing to environmental sustainability and resource recovery.

The primary objective of this study is to develop and characterize ZnO-modified hydrochar derived from paper waste sludge (PWSH@ZnO) for enhanced NH_4^+ removal from aqueous solutions. This modification aims to enhance NH_4^+ removal efficiency from aqueous solutions. The study evaluates the impact of ZnO loading on hydrochar's surface area, porosity, and functional groups, which are critical for adsorption performance. The study investigates the adsorption behavior of ZnO-modified hydrochar under various operational conditions, including pH, contact time, and initial NH_4^+ concentration. The analysis includes adsorption kinetics and isotherms to elucidate the underlying adsorption mechanisms. A key focus is to compare the performance of ZnO-modified hydrochar with

unmodified hydrochar, demonstrating the enhancements in adsorption capacity and efficiency due to ZnO modification. This work addresses pressing environmental challenges by utilizing paper waste sludge, offering a sustainable solution for NH_4^+ removal in wastewater treatment. The findings are expected to contribute to developing cost-effective and eco-friendly materials for environmental remediation.

Materials and methods

Material preparation

The paper waste sludge (PWS) was collected from the primary clarifier of the Hoang Van Thu Paper Joint Stock Company's pulp wastewater treatment facility in Thai Nguyen City, Vietnam. The collected PWS was air-dried under sunlight for three days and then oven-dried at 105 °C for 48 hours to ensure complete moisture removal. The dried PWS was then subjected to hydrothermal carbonization in a Teflon-lined stainless steel autoclave to produce hydrochar. A mixture of 10.0 g dried PWS and 40.0 mL of 0.25 M NaOH solution was prepared in a 300 mL Teflon vessel. The vessel was heated in an electric furnace at 10 °C min^{-1} to 200 °C and maintained at this temperature for 24 hours before cooling to room temperature.[1] After hydrothermal treatment, the liquid phase was separated from the solid residue using a 0.45 μm membrane filter. The solid residue was washed three times with distilled water to remove residual chemicals and then dried at 105 °C for two hours. The dried hydrochar was mechanically crushed and sieved to obtain particles with a diameter of less than 0.5 mm. The resulting hydrochar, designated as PWSH, was stored in a sealed glass container for further use.

ZnO nanoparticle synthesis. The ZnO-NPs were synthesized electrochemically using zinc electrodes (>90% purity) and a 0.5 M chloride solution as the electrolyte. The experimental setup was immersed in a water bath maintained at 30–50 °C. A 10 V voltage was applied using a DC power supply (model TES-6220). The system was continuously stirred at 400 rpm using a magnetic stirrer to ensure uniform reaction conditions. After 60 minutes, the ZnO-NP suspension was collected and cooled to room temperature (~25 °C). The cooled mixture was filtered through a 0.2 μm polyvinylidene difluoride membrane to control particle size. The filtered suspension was dried at 80 °C for 12 hours, yielding ZnO-NPs ready for further use.

Synthesis of PWSH@ZnO composite. The PWSH@ZnO composite was synthesized using the incipient wetness impregnation technique. Measured amounts of ZnO-NPs were added to 250 mL heat-resistant Erlenmeyer flasks containing 40 mL of ethanol. The mixture was sonicated for 30 minutes to ensure thorough nanoparticle dispersion. After sonication, predetermined amounts of PWSH were added to achieve ZnO-to-PWSH weight ratios of 5%, 10%, and 15%. The flasks were sealed and stirred at 80 °C for 2 hours using a magnetic stirrer (VELP, SN: F20500162, Italy). After the reaction, the suspension was filtered and rinsed with distilled water until a neutral pH was achieved. The filtered material was dried at 105 °C for 2 hours, yielding ZnO-impregnated hydrochar.

Batch adsorption experiment

The effects of initial solution pH and ZnO-NPs-to-PWSH mass ratio on NH_4^+ adsorption by PWSH and PWSH@ZnO were investigated through batch experiments. Batch experiments were conducted in 50 mL Erlenmeyer flasks containing 25 mL of a 20 mg L^{-1} NH_4^+ solution and 2 g L^{-1} adsorbent. The flasks were sealed with paraffin and shaken at 120 rpm for 60 minutes at 25 ± 2 °C using a shaker (PH-4A, China).

Subsequent investigations were conducted to explore the influence of contact time and adsorption kinetics, based on the initial solution pH and the mass ratio of ZnO to PWSH, which were determined in earlier experiments. These studies were carried out over a range of time intervals (5 to 240 minutes), with an initial NH_4^+ concentration of 20 mg L^{-1} and an adsorbent dosage of 2 g L^{-1}. The adsorbents used were either PWSH or PWSH@ZnO, and the experiments were performed at the optimal pH for NH_4^+ adsorption.

The effects of initial NH_4^+ concentrations and adsorption isotherms were investigated by mixing either PWSH or PWSH@ZnO at a dosage of 2 g L^{-1} with 25 mL of NH_4^+ solutions, with concentrations ranging from 10 to 100 mg L^{-1}. The mixtures were agitated at 120 rpm under optimal conditions for solution pH, mass ratio of ZnO to PWSH, and contact time, as determined in previous experiments.

The pH of the initial solutions was adjusted using 0.1 M hydrochloric acid (HCl) and 0.1 M sodium hydroxide (NaOH) solutions. After adsorption, the mixtures were filtered using filter paper with a pore size of 0.11 μm. The concentration of residual NH_4^+ in the supernatant was quantified using a UV/Vis spectrophotometer (Shimadzu, model Z2000, Japan) at a wavelength of 640 nm. Each experiment was conducted in triplicate to ensure reproducibility and accuracy of the results.

The adsorption capacity of NH_4^+ onto PWSH and PWSH@ZnO at time t (q_t, mg g^{-1}) and at equilibrium (q_e, mg g^{-1}) was determined using the following equations:

$$q_e = \frac{(C_0 - C_e)V}{M} \quad (1)$$

$$q_t = \frac{(C_0 - C_t)V}{M} \quad (2)$$

where C_0, C_t and C_e (mg L^{-1}) are concentrations of NH_4^+ at beginning time, any time t, and equilibrium, respectively; V (L) is the working volume of NH_4^+ solution; W (g) is the dry weight of ZnO/hydrochar absorbent.

Adsorption isotherm and kinetic models

Two widely recognized models, namely the pseudo-first-order and pseudo-second-order models, were employed to characterize the kinetics of NH_4^+ adsorption onto PWSH and PWSH@ZnO. The equations representing these two models are provided below:

$$\ln(q_e - q_t) = \ln q_e - k_1 t \quad (3)$$

$$\frac{t}{q_t} = \frac{1}{k_2 q_e^2} + \frac{1}{q_e} t \quad (4)$$

where q_e, q_t (mg g^{-1}) are the adsorption capacity at equilibrium and at time t (min), respectively; k_1 (min^{-1}) and k_2 (g mg^{-1} min^{-1}) are the rate constant of the pseudo-first-order and pseudo-second-order models, respectively;

The Langmuir and Freundlich models were employed to elucidate the adsorption isotherms of NH_4^+ onto PWSH and PWSH@ZnO. The Langmuir model posits that the adsorption process occurs on a monolayer surface, where the energy of the active sites remains constant. In contrast, the Freundlich model suggests that sorption occurs on a heterogeneous surface with varying energy levels of the active sites. The corresponding equations for the Langmuir and Freundlich models are presented as eqn (5) and (6), respectively:

$$q_e = \frac{q_m K_L C_e}{1 + K_L C_e} \quad (5)$$

$$q_e = K_F C_e^{1/n} \quad (6)$$

where q_e, q_m (mg g^{-1}) are the equilibrium and maximum adsorption capacity, respectively; C_e (mg L^{-1}) is the concentration of NH_4^+ in solution; K_L (L mg^{-1}) is the Langmuir constant; K_F (mg g^{-1}) is the Freundlich constant and n is the adsorption intensity.

Results and discussion

Characteristics of PWSH and PWSH@ZnO

SEM analysis of pristine PWSH and PWSH@ZnO provides insights into their structural and functional characteristics for NH_4^+ adsorption in water pollution treatment. The SEM image of pristine PWSH (Fig. 1a) shows a heterogeneous surface with large, rough particles and poorly defined pores. This morphology indicates that PWSH retains its original surface characteristics after hydrothermal treatment, which is crucial for its adsorption capabilities. The low porosity suggests a limited surface area, potentially reducing its adsorption capacity compared to modified materials.[26] In contrast, the SEM image of PWSH@ZnO (Fig. 1b) reveals increased surface roughness, attributed to the distribution of ZnO nanoparticles on the PWSH surface. This observation is supported by FESEM images of ZnO-NPs (Fig. 1e). The morphological analysis reveals a porous, irregular surface with a uniform distribution of

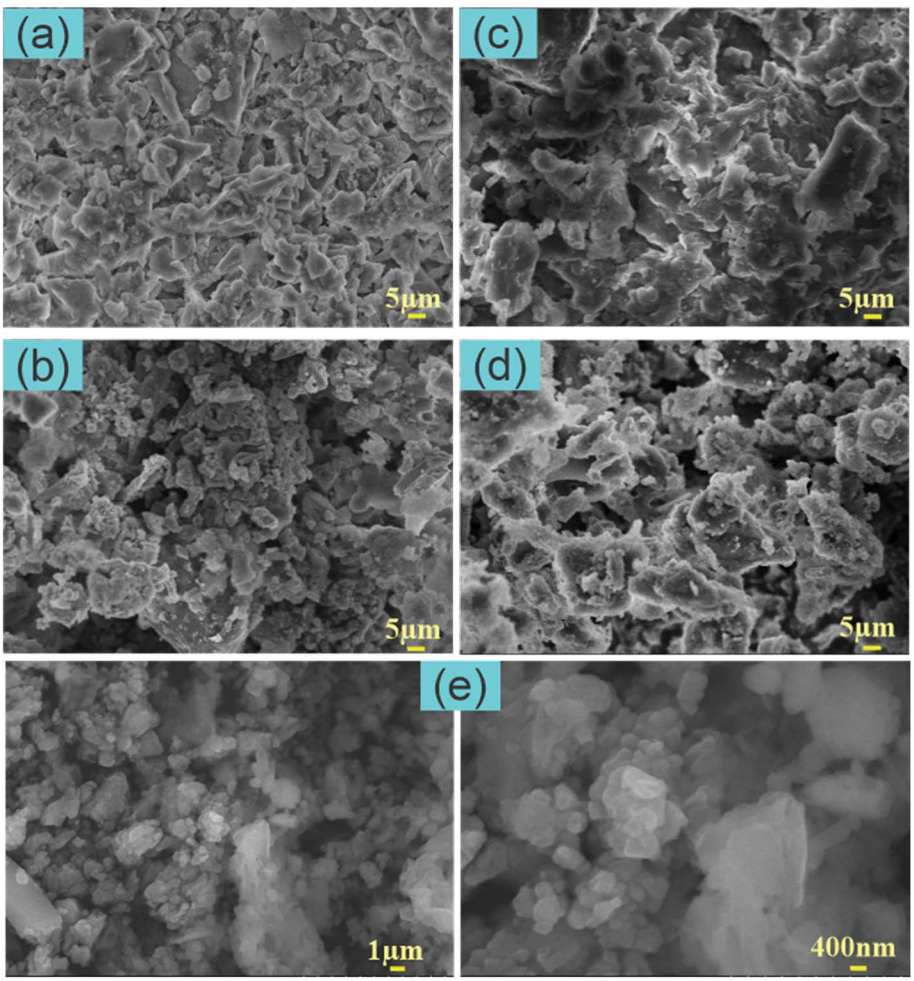

Fig. 1 SEM image of PWSH (a), PWSH@ZnO (b), PWSH after NH_4^+ adsorption (c), PWSH@ZnO after NH_4^+ adsorption (d) and FESEM images of ZnO-NPs (e).

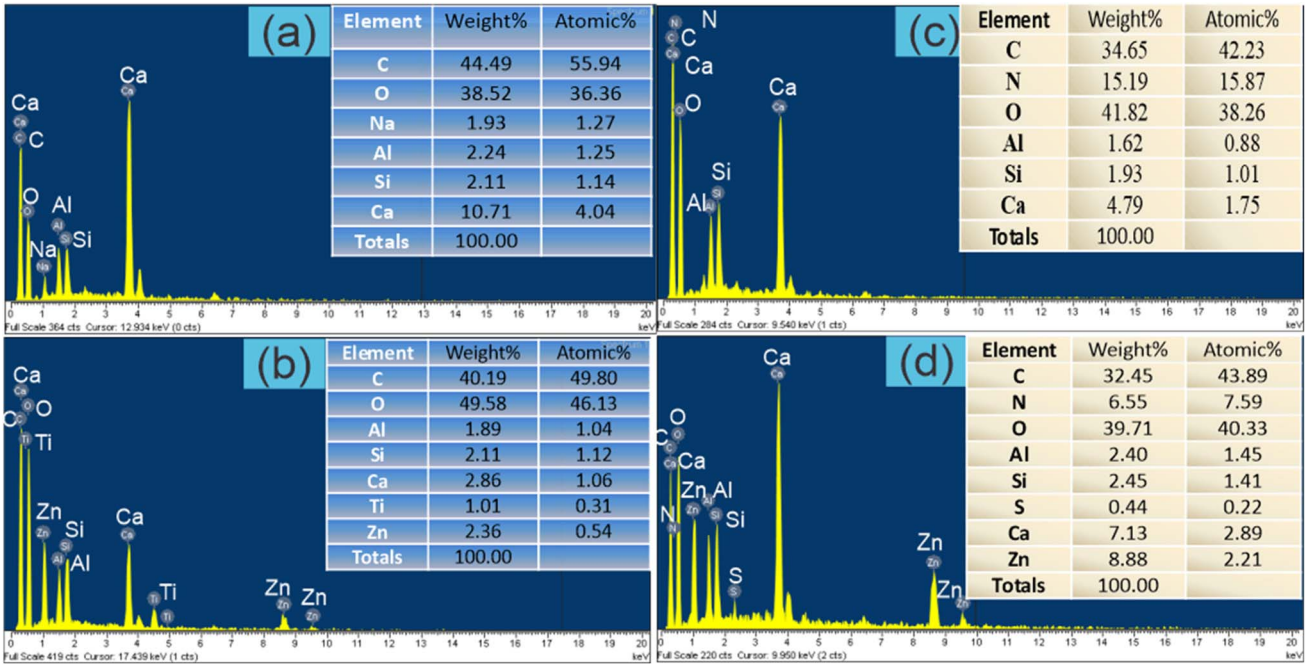

Fig. 2 EDX spectra PWSH (a), PWSH@ZnO (b), PWSH after NH_4^+ adsorption (c) and PWSH@ZnO after NH_4^+ adsorption (d).

ultrafine particles. The presence of ZnO nanoparticles is confirmed by EDX analysis (Fig. 2b). These nanoparticles provide additional adsorption sites, enhancing the material's efficiency in removing pollutants, including organic compounds and metal ions, from aqueous environments.[27] The synergistic adsorption effect in PWSH@ZnO enhances its contaminant removal efficiency, making it a promising candidate for wastewater treatment.

The SEM image of PWSH after NH_4^+ adsorption (Fig. 1c) shows significant changes in surface morphology, characterized by the formation of aggregated particles and smoother regions. These alterations are likely due to the deposition of NH_4^+ ions on the PWSH surface, suggesting a strong interaction between the NH_4^+ ions and the functional groups on the PWSH material. This interaction enhances the material's adsorption capacity, as supported by findings that highlight the role of functional groups on adsorbents in ion adsorption processes.[28] Furthermore, the adsorption mechanisms emphasize the importance of surface characteristics in determining ion removal efficiency from aqueous solutions.[29] In contrast, the SEM image of PWSH@ZnO after NH_4^+ adsorption (Fig. 1d) reveals a distinct surface morphology compared to PWSH. The ZnO particles remain visible even after adsorption, indicating that the PWSH@ZnO composite can effectively adsorb NH_4^+ while preserving the structural integrity of the ZnO particles. This characteristic is crucial for enhancing the material's reusability, as ZnO nanostructures have been shown to exhibit good regeneration and reusability without significant loss of sorption capacity.[30] The synergistic effect of adsorption and photocatalytic properties of ZnO further contributes to pollutant removal from water, underscoring the dual functionality of ZnO in both adsorption and photocatalysis.[25]

The superior adsorption capacity of PWSH@ZnO compared to pristine PWSH can be attributed to the increased surface area provided by the ZnO nanoparticles, which introduce additional adsorption sites. This finding aligns with previous research, which reported that incorporating ZnO nanoparticles significantly enhances the adsorption capacity of composite materials.[31] Moreover, the structural changes observed after NH_4^+ adsorption in both samples indicate a strong interaction between the materials and NH_4^+, with the interaction in PWSH@ZnO likely being further enhanced by the presence of ZnO. This is supported by studies highlighting the role of ZnO in improving the adsorption characteristics of composite materials.[32]

EDX spectra provide critical insights into the elemental composition of PWSH, PWSH@ZnO, and their NH_4^+ adsorbed forms. The analysis reveals significant changes in elemental composition, correlating with adsorption processes. The EDX spectrum of PWSH (Fig. 2a) shows a predominance of C (44.49 wt%, 55.94 at%), highlighting its organic nature. O is present at 38.52 wt% and 36.36 at%, indicating oxygen-containing functional groups that enhance adsorption capabilities.[33] Ca (10.71 wt%, 4.04 at%) indicates inorganic compounds from the raw paper sludge, while minor elements like Na, Al, and Si contribute to the composition.[34] This elemental distribution aligns with studies highlighting the role of functional groups in hydrochar adsorption.[35] For PWSH@ZnO (Fig. 2b), the EDX spectrum shows increased O content (49.58 wt%, 46.13 at%), attributed to ZnO-NPs, which contribute significantly to the oxygen content.[36] The presence of Zn (2.36 wt%, 0.54 at%) confirms the successful modification of PWSH with ZnO, enhancing adsorption properties due to its high surface area and active sites.[37] The decrease in C content to

40.19 wt% indicates a dilution effect from ZnO-NPs. Meanwhile, Ca and other elements remain stable, indicating that the modification primarily affects C and O content without significantly altering the hydrochar's inherent composition.[38]

After NH_4^+ adsorption, the EDX spectrum of PWSH (Fig. 2c) shows a notable reduction in carbon (C) content to 34.65% by weight (42.23% atomic), likely due to the introduction of nitrogen (N) at 15.19% by weight (15.87% atomic), confirming the successful adsorption of NH_4^+ ions. The oxygen (O) content remains stable at 41.83%, indicating that the oxygen-containing functional groups are preserved during the adsorption process. The decrease in calcium (Ca) to 4.79% by weight suggests possible interactions or displacements between Ca and NH_4^+ ions, consistent with ion exchange behavior in adsorption processes.[39] In contrast, the EDX spectrum of PWSH@ZnO after NH_4^+ adsorption (Fig. 2d) shows further changes, with carbon content decreasing to 32.45% by weight (43.89% atomic) and nitrogen increasing to 6.55% by weight (7.59% atomic), indicating effective NH_4^+ uptake.[40] Notably, the zinc (Zn) content rises significantly to 7.13% by weight (2.89% atomic), suggesting that ZnO not only remains on the surface but may also enhance NH_4^+ adsorption through favorable interactions with nitrogen compounds.[41] The O content remains high at 39.71%, reflecting the retention of the modified properties of the material even after adsorption.

The analysis of PWSH and PWSH@ZnO using BET analysis, FTIR spectra and the point of zero charge (pH_{PZC}) provides valuable insights into their surface characteristics, chemical functionalities, and adsorption behaviors, which are crucial for their application in environmental remediation. The BET analysis reveals significant differences in the surface areas of PWSH and PWSH@ZnO. The surface area of pristine PWSH is

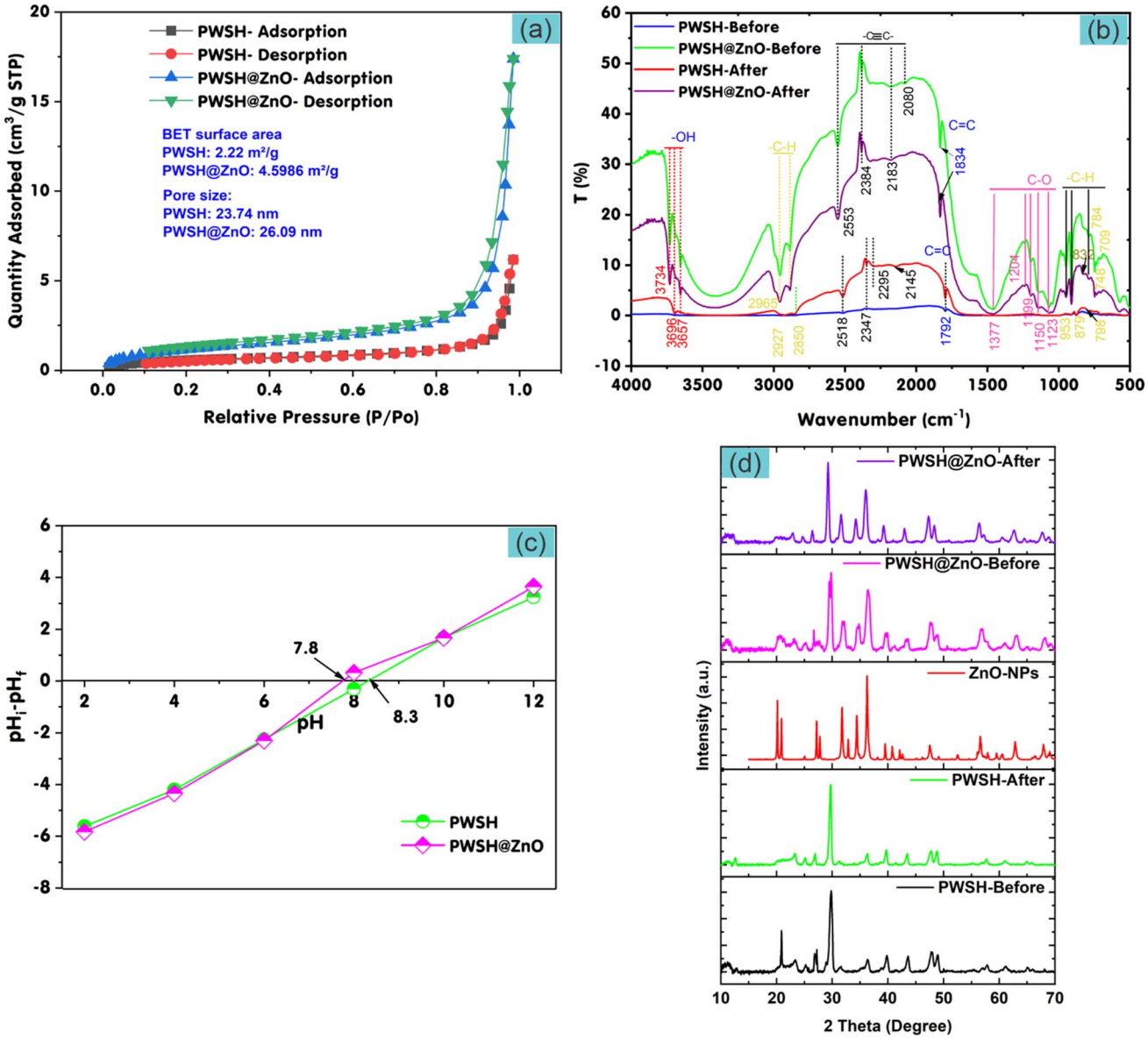

Fig. 3 BET analysis (a), FTIR (b), pH_{PZC} (c) and XRD patterns (d) of PWSH and PWSH@ZnO.

measured at 2.2 $m^2 g^{-1}$, indicating low porosity. Meanwhile, the pore sizes of PWSH and PWSH@ZnO are similar, measuring 23.74 nm and 26.09 nm, respectively. The isotherm curves for PWSH exhibit typical Type IV behavior, indicative of a mesoporous structure (Fig. 3a). In contrast, the BET surface area of PWSH@ZnO is measured at 4.6 $m^2 g^{-1}$, which is relatively low, especially considering the expectation that ZnO nanoparticles would enhance the material's porosity. This observation can be attributed to several factors. Firstly, the BET analysis shows that pristine PWSH has a low surface area, suggesting that the material inherently possesses low porosity. Upon modification with ZnO, the surface area increases to 4.6 $m^2 g^{-1}$, indicating a modest enhancement in porosity. This increase is consistent with the introduction of ZnO nanoparticles, which can either create new pores or expand existing ones, thus providing additional active sites for adsorption. However, the relatively small increase in surface area may be explained by several factors. It is possible that the ZnO nanoparticles were not uniformly distributed across the hydrochar surface, limiting their effectiveness in enhancing porosity. Additionally, the deposition of ZnO nanoparticles may have partially blocked or filled some of the pores in the hydrochar, preventing a significant increase in surface area. These factors may explain why the surface area, although higher than that of pristine PWSH, remains relatively low compared to other materials that typically exhibit a more pronounced enhancement of porosity following ZnO modification.[42]

The FTIR spectra analysis before and after NH_4^+ adsorption on PWSH and PWSH@ZnO surfaces (Fig. 3b) reveals significant changes in the vibrational peaks, which indicate interactions between functional groups and the adsorbate. Initially, the PWSH@ZnO sample exhibits a broad peak in the 3500–3600 cm^{-1} range, characteristic of hydroxyl (–OH) stretching, suggesting a significant presence of hydroxyl groups on the surface. This observation aligns with studies highlighting the role of hydroxyl groups in enhancing adsorption properties through the formation of hydrogen bonds with adsorbates. The peak around 1600 cm^{-1}, associated with carbonyl (C=O) groups, is more pronounced in PWSH@ZnO, suggesting a stronger interaction between PWSH and ZnO, which may facilitate the adsorption process.[43] In contrast, the PWSH sample shows similar peaks but with reduced intensity, likely due to the absence of ZnO, which is known to enhance the interaction between NH_4^+ ions and surface functional groups. The presence of ZnO not only increases the number of available adsorption sites but also modifies the electronic environment of the surface, thereby improving the overall adsorption capacity.

After NH_4^+ adsorption, both samples show significant changes in their FTIR spectra. The hydroxyl peak shifts to lower wavenumbers (~3400 cm^{-1}), suggesting hydrogen bond formation between NH_4^+ ions and hydroxyl groups. This shift is more pronounced in PWSH@ZnO, indicating stronger interactions due to ZnO, which enhances NH_4^+ binding affinity.[44] The carbonyl peak may also shift or change in intensity, indicating NH_4^+ interaction with carbonyl groups, possibly through complex formation or direct adsorption. Peaks associated with C–O and C–H stretching (1100–1200 cm^{-1}) may decrease in intensity after NH_4^+ adsorption, reflecting structural changes in these functional groups. The shifts and intensity changes in hydroxyl, carbonyl, and C–O peaks provide strong evidence of the role of surface functional groups in adsorption. The enhanced interactions in PWSH@ZnO highlight ZnO's critical role in facilitating adsorption, confirming the NH_4^+ adsorption mechanism. FTIR analysis elucidates the interactions between NH_4^+ ions and functional groups on PWSH and PWSH@ZnO surfaces. The pronounced spectral changes in hydroxyl and carbonyl regions affirm the significant role of these functional groups in adsorption, with ZnO enhancing these interactions.

The point of zero charge (pH_{PZC}) analysis is crucial for understanding the surface charge behavior of the materials under varying pH conditions. PWSH has a pH_{PZC} of approximately 7.8 (Fig. 3c), indicating that it exhibits a net positive charge below this pH and a net negative charge above it. This property suggests that PWSH is more effective at adsorbing anions in acidic conditions and cations in basic conditions. In contrast, PWSH@ZnO has a slightly higher pH_{PZC} of 8.3 (Fig. 3c), indicating that its surface becomes positively charged at a higher pH than PWSH. This increase in pH_{PZC} can be attributed to the presence of ZnO nanoparticles, which likely introduce additional hydroxyl groups, altering the surface chemistry and enhancing the material's ability to interact with different ions depending on the solution pH.[33] This shift in pH_{PZC} indicates that ZnO modification enhances the versatility and efficiency of PWSH@ZnO as an adsorbent under various environmental conditions, making it particularly suitable for applications in wastewater treatment.

The X-ray diffraction (XRD) patterns of PWSH and PWSH@ZnO, both before and after NH_4^+ adsorption, provide valuable insights into the crystallinity and stability of the ZnO nanoparticles integrated within the hydrochar matrix (Fig. 3d). Prior to NH_4^+ adsorption, the XRD pattern of PWSH exhibits several characteristic peaks indicative of its predominantly amorphous structure. Notably, a broad peak at $2\theta = 22°$ is typical of amorphous carbon, a common feature of hydrochar materials.[45] Additionally, a peak at $2\theta = 28.4°$ corresponds to the (101) plane of disordered carbon within PWSH. Other peaks at 2θ values of 29.7°, 36.2°, 39.7°, 43.6°, 47.7°, and 27.2° further confirm the presence of disordered or low-crystallinity carbon, as well as potentially some oxygenated functional groups, such as hydroxyl or carboxyl groups, which are commonly found in hydrochars.[46] These broad, diffuse peaks support the idea that PWSH is primarily composed of an amorphous carbon matrix, with minor impurities or residual minerals.

Following NH_4^+ adsorption, significant alterations are observed in the XRD pattern of PWSH. Notably, the peak at $2\theta = 20.9°$, which was present prior to adsorption, disappears after the adsorption process. This suggests that the interaction with NH_4^+ ions induces modifications in the local carbon structure, potentially altering the disorder or functional groups within the material. Despite this change, several other peaks, including those at $2\theta = 22°$, 28.4°, 29.7°, 36.2°, 39.7°, 43.6°, 47.7°, and 27.2°, remain intact, indicating that the overall amorphous structure of PWSH is largely preserved after NH_4^+ adsorption, with only minor changes occurring due to the adsorption

process. The disappearance of the $2\theta = 20.9°$ peak suggests a localized alteration, yet the material retains its overall amorphous characteristics.

The presence of ZnO particles is distinctly evidenced by eight prominent diffraction peaks observed at 31.7°, 34.4°, 36.2°, 56.6°, 62.8°, 66.3°, 67.9° and 69.0° in the XRD pattern of ZnO nanoparticles (Fig. 3d).[47] Notably, the XRD pattern of PWSH@ZnO prior to NH_4^+ adsorption displays sharp, well-defined peaks characteristic of crystalline ZnO. These peaks, located at 2θ values of 31.7°, 34.4°, 36.2°, 47.5°, 56.5°, 62.8°, 66.3° and 68.0°, correspond to the hexagonal wurtzite structure of ZnO (JCPDS no. 36-1451),[48] confirming the well-crystallized nature of the ZnO nanoparticles. The sharpness of these diffraction peaks underscores the high crystallinity of the ZnO phase within the composite, further supporting the successful incorporation of ZnO into the hydrochar matrix and demonstrating the effective integration of ZnO within the PWSH composite.

After NH_4^+ adsorption, the XRD pattern of PWSH@ZnO remains largely unchanged. The characteristic ZnO peaks persist, with no significant shifts in 2θ values or peak intensities, indicating that the ZnO nanoparticles retain their crystalline structure even after interacting with NH_4^+ ions. This stability suggests that NH_4^+ adsorption does not induce any major alterations in the ZnO lattice or cause its degradation. Such stability is crucial for the sustained performance of PWSH@ZnO in practical applications, as it ensures that the material maintains its structural integrity during the adsorption of ammonium ions.[49]

Effect of ZnO nanoparticles modification ratio

The investigation into the impact of ZnO nanoparticle (ZnO-NPs) modification on the synthesis of PWSH@ZnO for NH_4^+ adsorption capacity reveals significant findings. The adsorption experiments were conducted under controlled conditions, with an initial NH_4^+ concentration of 20 mg L^{-1}, solution pH of 6.28 and an adsorbent dosage of 2 g L^{-1}, with a contact time of 60 minutes. The study systematically examined the modification of hydrochar with varying ZnO-NP ratios (5%, 10%, and 15% w/w) to assess their effects on NH_4^+ removal efficiency and adsorption capacity.

The results revealed a clear trend where both the adsorption capacity (q) and removal efficiency (H) increased with higher ZnO-NP ratios (Fig. 4). Specifically, the removal efficiency for PWSH alone was recorded at 64.21%, with an adsorption capacity of 6.42 mg g^{-1}. Upon introducing 5% ZnO-NPs, the removal efficiency increased to 70.82%, and the adsorption capacity rose to 7.08 mg g^{-1}. The most significant enhancement was observed at 10% ZnO-NPs, where the removal efficiency reached 82.87%, corresponding to an adsorption capacity of 8.29 mg g^{-1}. However, at 15% ZnO-NPs, the performance improvements were marginal, with a removal efficiency of 83.18% and an adsorption capacity of 8.32 mg g^{-1}. This pattern indicates a positive correlation between ZnO-NP ratios and both adsorption capacity and removal efficiency, particularly up to the 10% modification threshold.

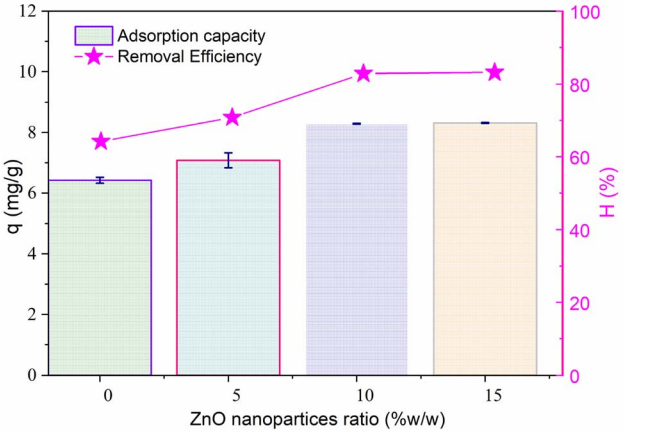

Fig. 4 The effect of the ratio of ZnO nanoparticle modification to hydrothermal paper sludge biochar (PWSH@ZnO) on NH_4^+ adsorption efficiency; experimental conditions: initial NH_4^+ concentration 20 mg L^{-1}; adsorbent dosage 2 g L^{-1} and pH 8, contact time of 60 min.

The enhanced adsorption performance can be attributed to the increased surface area and reactivity of the hydrochar due to the incorporation of ZnO-NPs, which provide additional active sites for NH_4^+. The mechanisms of ion exchange and surface complexation, facilitated by ZnO-NPs, further enhance the material's affinity for NH_4^+, thereby improving overall removal efficiency.[24,50] However, the diminishing returns observed beyond the 10% modification level suggest that the saturation of active sites on the adsorbent surface limits further improvements in adsorption capacity and efficiency. This finding is consistent with previous studies, which have indicated optimal nanoparticle loading levels for modified adsorbents, where excessive amounts may not provide proportional benefits.[51,52]

The data suggest that a 10% ZnO-NPs modification is optimal for maximizing NH_4^+ removal, achieving high removal efficiency without the diminishing returns observed at higher concentrations. The optimal ZnO loading of 10% in PWSH@ZnO for NH_4^+ adsorption can be attributed to several interrelated factors. At this concentration, ZnO nanoparticles are effectively dispersed across the surface of the hydrochar, leading to an increased number of active sites available for NH_4^+ adsorption. This enhanced dispersion results in a significant improvement in both the adsorption capacity and removal efficiency of NH_4^+ ions from the solution. However, when the ZnO concentration exceeds 10%, a saturation effect is likely to occur. For example, at a 15% ZnO loading, the available active sites for NH_4^+ adsorption may become limited as ZnO nanoparticles begin to agglomerate or form larger clusters. This clustering phenomenon reduces the overall surface area available for adsorption and may block some active sites, thereby diminishing both adsorption capacity and removal efficiency. Additionally, at higher ZnO concentrations, steric hindrance may arise, where the nanoparticles' surfaces partially cover the active adsorption sites on the hydrochar surface, hindering interactions between NH_4^+ ions and the hydrochar material. These steric effects further contribute to the observed reduction

in adsorption efficiency at elevated ZnO loadings. This optimal ratio balances material efficiency with performance, indicating that the composite material of paper sludge-derived hydrochar and ZnO-NPs presents a sustainable and cost-effective solution for NH_4^+ adsorption. The results highlight the potential application of this composite in large-scale wastewater treatment, capitalizing on its high performance and low-cost raw materials.

Effect of solution pH on NH_4^+ adsorption

The effect of pH on the NH_4^+ adsorption efficiency and capacity of PWSH and PWSH@ZnO is illustrated in Fig. 5. Adsorption experiments were conducted under controlled conditions, with an initial NH_4^+ concentration of 20 mg L^{-1} and an adsorbent dose of 2 g L^{-1} over a contact time of 60 minutes. The pH of the solution was varied from 4 to 11 to investigate the influence of pH on the adsorption performance.

The adsorption capacity and removal efficiency of PWSH were significantly influenced by the pH of the solution (Fig. 5a). At pH 4, both removal efficiency and adsorption capacity were relatively low, recorded at 46.66% and 4.67 mg g^{-1}, respectively. As the pH increased, both parameters gradually improved, peaking at pH 8 with a removal efficiency of 68.03% and an adsorption capacity of 6.80 mg g^{-1}. However, beyond this point, both the removal efficiency and adsorption capacity experienced a slight decline, with values of 66.62% and 6.66 mg g^{-1} at pH 10. This trend can be attributed to the ionization state of NH_4^+ and the surface charge characteristics of the adsorbent. At lower pH values, the higher concentration of H^+ ions may lead to competition between H^+ and NH_4^+ ions for adsorption sites on the hydrochar surface. As the pH increases, the concentration of NH_4^+ ions becomes more stable, enhancing their interaction with the adsorbent surface and leading to improved adsorption. However, at pH levels above 8, the formation of NH_3 (ammonia gas) becomes more pronounced, which may reduce overall adsorption efficiency, as NH_3 is less likely to adsorb onto the surface.[53–55]

PWSH@ZnO exhibited superior adsorption performance across the entire pH range studied (Fig. 5b). PWSH@ZnO showed significantly higher removal efficiency and adsorption capacity than unmodified PWSH. At pH 4, the removal efficiency was relatively low but higher than that of unmodified PWSH, indicating that ZnO-NPs enhance adsorption even under acidic conditions. At pH 4, the adsorption capacity was 4.67 mg g^{-1}, with a removal efficiency of 46.66%. As pH increased, adsorption capacity and removal efficiency improved significantly. At pH 8, the removal efficiency reached 68.03%, with an adsorption capacity of 6.80 mg g^{-1}, indicating optimal performance. This trend suggests that at pH 8, NH_4^+-PWSH@ZnO interactions are maximized, likely due to electrostatic attraction between the negatively charged PWSH@ZnO surface and NH_4^+ ions. At pH 9 and 10, PWSH@ZnO maintained high adsorption performance. At pH 9, the removal efficiency increased slightly to 68.33%, with an adsorption capacity of 6.83 mg g^{-1}. At pH 10, the removal efficiency remained high at 66.62%, with an adsorption capacity of 6.66 mg g^{-1}. This stability at higher pH levels indicates that PWSH@ZnO is less affected by NH_4^+-to-NH_3 conversion compared to unmodified PWSH, which shows a more significant performance decline under similar conditions.[32,56]

The superior performance of PWSH@ZnO can be attributed to several key factors. First, the incorporation of ZnO nanoparticles increases the surface area of the hydrochar, providing additional active sites that enhance the interaction between NH_4^+ ions and the adsorbent. Second, ZnO is known for its catalytic properties, which may accelerate adsorption kinetics, particularly under higher pH conditions. At elevated pH, the surface of ZnO becomes negatively charged, which favors the adsorption of positively charged NH_4^+ ions through electrostatic attraction. PWSH, characterized by a negative zeta potential of −7.3 mV (Fig. 5a), benefits from this negative charge, facilitating NH_4^+ adsorption *via* electrostatic forces. In contrast, PWSH@ZnO, with the addition of zinc oxide, exhibits a positive zeta potential of +6.5 mV (Fig. 5b). This positive charge

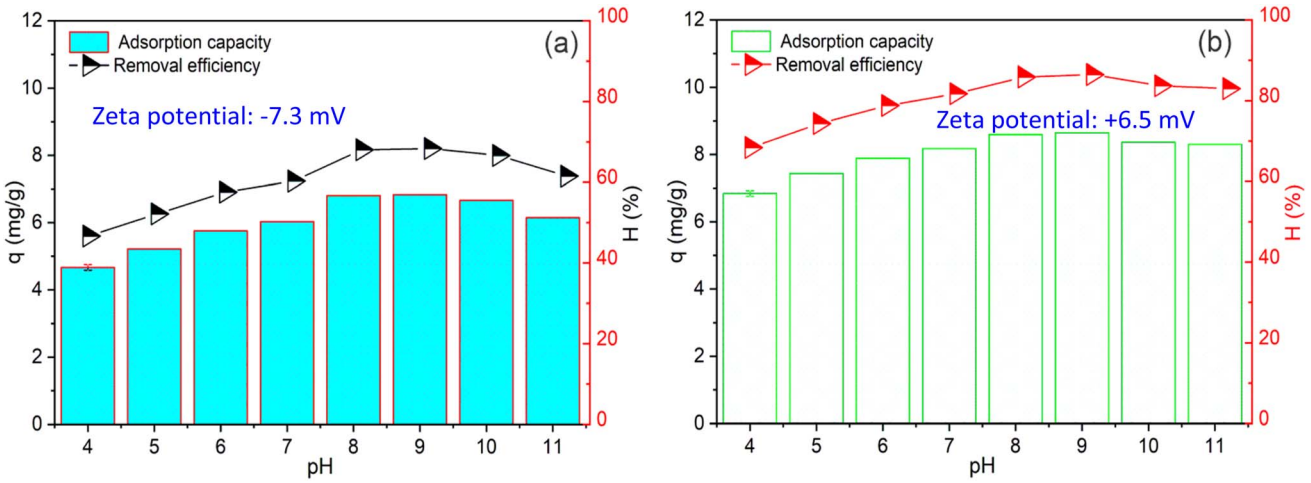

Fig. 5 The effect of pH solution on NH_4^+ adsorption efficiency using PWSH (a) and PWSH@ZnO (b); experimental conditions: initial NH_4^+ concentration 20 mg L^{-1}; adsorbent dosage 2 g L^{-1}, contact time of 60 min.

enhances the electrostatic attraction toward NH_4^+ ions, significantly improving its adsorption capacity compared to PWSH alone. This mechanism is less effective in PWSH due to the absence of ZnO nanoparticles.[57,58] The experimental results indicate that pH 8 is optimal for NH_4^+ adsorption in both PWSH and PWSH@ZnO. At this pH, PWSH achieved a maximum removal efficiency of 68.03% and an adsorption uptake of 6.80 mg g^{-1}. Similarly, PWSH@ZnO exhibited its best performance at pH 8, with a significantly higher removal efficiency of 80.00% and an adsorption uptake of 10.00 mg g^{-1}. These findings highlight that while both materials perform optimally at pH 8, the ZnO nanoparticle modification substantially enhances both the adsorption capacity and removal efficiency of the composite, making it a more effective adsorbent compared to unmodified PWSH.

These results indicate that modifying PWSH with ZnO nanoparticles significantly improves its adsorption properties, leading to a higher adsorption capacity and enhanced stability across a wider pH range. The incorporation of ZnO-NPs increases the number of available active sites and surface area, which contributes to more efficient adsorption of NH_4^+ ions. Moreover, ZnO facilitates stronger electrostatic interactions with NH_4^+, particularly in alkaline conditions, where PWSH alone experiences reduced efficiency. Consequently, PWSH@ZnO proves to be a more versatile and effective adsorbent for NH_4^+ removal across different pH environments.

Effect of adsorption time and adsorption kinetics

The effect of adsorption time on NH_4^+ removal by PWSH and PWSH@ZnO was evaluated under controlled experimental conditions. The initial NH_4^+ concentration was set at 20 mg L^{-1}, with pH 8 optimized for NH_4^+ adsorption. The adsorbent dosage was 2 g L^{-1}, and contact times ranged from 5 to 240 minutes to analyze adsorption kinetics.

The adsorption behavior of both PWSH and PWSH@ZnO under varying contact times was thoroughly investigated. As contact time increased, both adsorption capacity and removal efficiency improved, eventually plateauing after a certain period. This is typical of adsorption processes, where the system approaches equilibrium as the available adsorption sites become saturated with NH_4^+ ions. Equilibrium for both PWSH and PWSH@ZnO was reached around 120 to 150 minutes (Fig. 6). After this point, the increase in adsorption capacity and removal efficiency was minimal, indicating that the majority of active sites had been occupied. For PWSH, the equilibrium adsorption capacity stabilized at approximately 7.52 mg g^{-1}, with a removal efficiency of around 75% (Fig. 6a). In contrast, PWSH@ZnO achieved a higher equilibrium adsorption capacity of 9.31 mg g^{-1}, with a removal efficiency of 93.19% (Fig. 6b), demonstrating its superior performance.

The accelerated approach to equilibrium in PWSH@ZnO suggests that the incorporation of ZnO-NPs enhances adsorption by increasing surface area and providing additional active sites for NH_4^+ ions. Notably, PWSH@ZnO exhibits a rapid adsorption rate, achieving over 80% removal efficiency within the first 60 minutes, which demonstrates its potential for applications requiring a quick response, such as in wastewater treatment systems.[53,59] The adsorption equilibrium for both materials is reached when their active sites become saturated. PWSH, with a limited number of active sites, shows a slower uptake and lower overall adsorption capacity. In contrast, PWSH@ZnO, benefiting from increased surface area and enhanced active sites from ZnO nanoparticles, reaches equilibrium more quickly and demonstrates a higher NH_4^+ uptake, making it a more efficient adsorbent.[60,61]

The improved performance of PWSH@ZnO is primarily due to the unique properties of ZnO nanoparticles, which enhance surface area and facilitate stronger electrostatic interactions with NH_4^+, especially at the optimal pH of 8. This pH range is critical for stabilizing NH_4^+ while minimizing NH_3 formation, which is less readily adsorbed.[57,62] These results highlight the potential of PWSH@ZnO as a highly effective and versatile adsorbent for NH_4^+ removal under various conditions, particularly in wastewater treatment applications where rapid adsorption is crucial.[63,64]

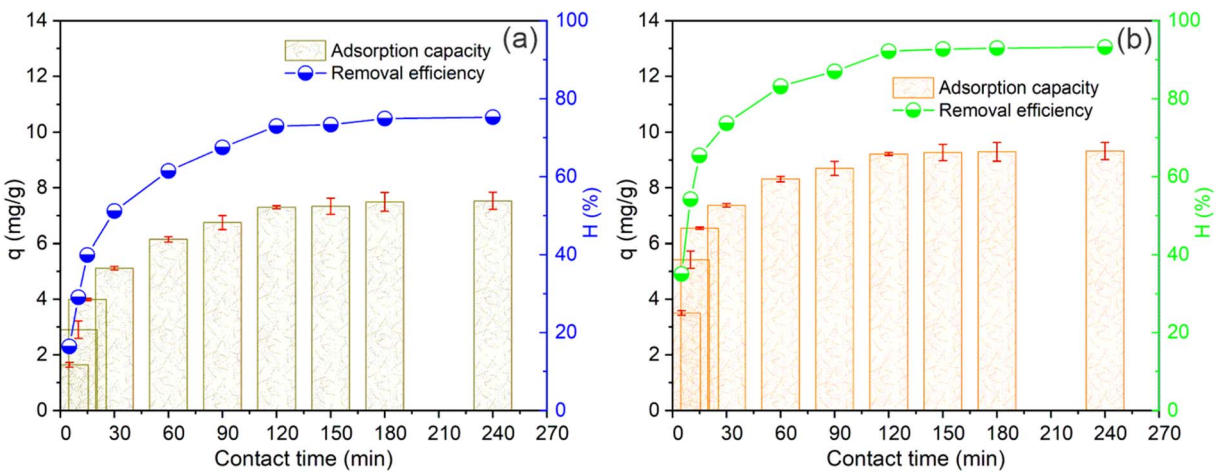

Fig. 6 Effect of contact time on the NH_4^+ adsorption efficiency using PWSH (a) and PWSH@ZnO (b) materials; experimental conditions: initial NH_4^+ concentration 20 mg L^{-1}; adsorbent dosage 2 g L^{-1}, pH 8.

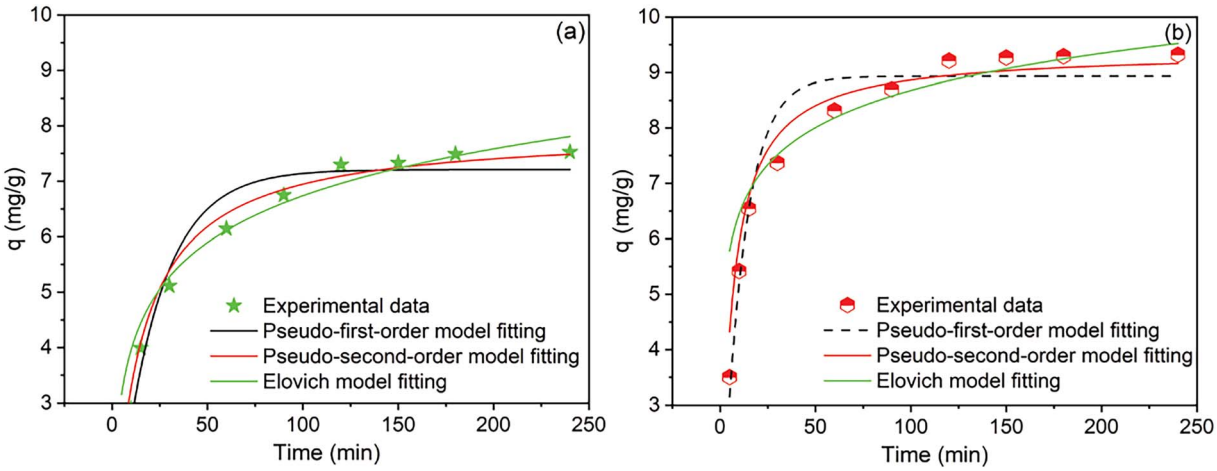

Fig. 7 Kinetic models of NH_4^+ adsorption by PWSH (a) and PWSH@ZnO (b); experimental conditions: initial NH_4^+ concentration 20 mg L^{-1}; adsorbent dosage 2 g L^{-1} and pH 8.

The kinetic modeling data for NH_4^+ adsorption onto PWSH and PWSH@ZnO are presented in Fig. 7 and summarized in Table 1. This study utilizes three well-established kinetic models: the pseudo-first-order, pseudo-second-order, and Elovich models. The primary objective is to identify the most appropriate kinetic model that best characterizes the adsorption process and to conduct a comprehensive analysis of the adsorption behavior of the materials.

The pseudo-first-order model posits that the adsorption rate is directly proportional to the number of available unoccupied sites on the adsorbent. For PWSH, the calculated adsorption capacity (q_e) is 7.21 mg g^{-1}, with a rate constant (k_1) of 0.046 min^{-1} and an R^2 value of 0.9747, indicating a strong fit of the model to the experimental data.[65] In contrast, PWSH@ZnO exhibits a higher adsorption capacity of 8.93 mg g^{-1} and a rate constant of 0.087 min^{-1}, but a lower R^2 value of 0.9480, suggesting that while the pseudo-first-order model is applicable, it does not fully describe the adsorption kinetics for PWSH@ZnO.[66]

The pseudo-second-order model, which assumes that the adsorption rate is proportional to the square of the number of unoccupied sites, is typically more applicable to systems dominated by chemisorption. For PWSH, this model predicts an adsorption capacity of 7.93 mg g^{-1} and a rate constant of 0.0089 g mg^{-1} min^{-1}, with an R^2 value of 0.9541 – slightly lower than that obtained with the pseudo-first-order model. For PWSH@ZnO, the pseudo-second-order model indicates a higher adsorption capacity of 9.38 mg g^{-1} and a rate constant of 0.018 g mg^{-1} min^{-1}, but the R^2 value of 0.9024 remains lower than that of the first-order model. This suggests that, although the pseudo-second-order model is applicable, it is less suitable for accurately describing the adsorption kinetics of PWSH@ZnO.[67]

The Elovich model is commonly used for systems with heterogeneous surfaces, particularly those involving chemisorption processes. For PWSH, the model parameters indicate an initial adsorption rate (α) of 2.245 mg g^{-1} min^{-1} and a desorption constant (β) of 0.766 mg g^{-1}, with a strong fit suggested by an R^2 value of 0.9556. In contrast, for PWSH@ZnO, the Elovich model predicts a significantly higher initial adsorption rate (α = 279.3 mg g^{-1} min^{-1}) and a desorption

Table 1 Parameters of the kinetic models for NH_4^+ adsorption using PWSH and PWSH@ZnO

Pseudo- first-order model			Pseudo-second-order model			
q_e (mg g^{-1})	k_1	R^2	$q_{m,cal}$ (mg g^{-1})	k_2	R^2	$q_{e,exp}$ (mg g^{-1})
PWSH						
7.21 ± 0.16	0.046 ± 0.002	0.9747	7.93 ± 0.01	0.0089 ± 0.0001	0.9541	9.21
PWSH@ZnO						
8.93 ± 0.19	0.087 ± 0.008	0.9480	9.38 ± 0.01	0.018 ± 0.0003	0.9024	

Elovich model					
PWSH			PWSH@ZnO		
α	β	R^2	α	β	R^2
2.245 ± 0.013	0.766 ± 0.01	0.9556	279.3 ± 65.33	1.199 ± 0.02	0.620

constant (β = 1.199 mg g^{-1}), but the R^2 value of 0.620 is considerably lower, indicating that the Elovich model is less suitable for describing the adsorption kinetics of PWSH@ZnO.[68]

The comparative analysis of the kinetic models reveals that for PWSH, the pseudo-first-order model provides the best fit, indicating that the NH_4^+ adsorption process is primarily governed by physisorption, where the availability of adsorption sites plays a central role in determining the adsorption rate.[69] For PWSH@ZnO, although the pseudo-first-order model also yields a relatively good fit, the slightly weaker correlation suggests that the introduction of ZnO nanoparticles may introduce additional complexities, such as chemisorption or surface heterogeneity, which this model does not fully account for.[70] The enhanced adsorption capacity and rate constants observed for PWSH@ZnO reflect the improved surface properties and the additional active sites provided by the ZnO nanoparticles.[71] While the Elovich model applies to PWSH, indicating surface heterogeneity and some chemisorption, its poor fit for PWSH@ZnO points to a more complex adsorption mechanism, likely involving a combination of physisorption and chemisorption that is not adequately described by the Elovich model.[72]

In summary, the adsorption kinetics of NH_4^+ on both PWSH and PWSH@ZnO are primarily governed by the pseudo-first-order model, particularly for PWSH, suggesting that physisorption is the dominant adsorption mechanism. However, the introduction of ZnO nanoparticles significantly enhances the material's adsorption efficiency. This improvement points to the involvement of more complex interactions, such as chemisorption or surface heterogeneity, which are not fully accounted for by traditional kinetic models.

Effect of ammonium concentration and adsorption isotherms

Fig. 8 illustrates the impact of initial NH_4^+ concentration on the adsorption capacity and removal efficiency of PWSH and PWSH@ZnO materials. The results show a consistent increase in adsorption capacity for both materials with rising NH_4^+ concentrations. For PWSH, the adsorption capacity rises from 3.86 mg g^{-1} at 10 mg L^{-1} to 18.38 mg g^{-1} at 100 mg L^{-1} (Fig. 8a). In contrast, PWSH@ZnO demonstrates a higher adsorption capacity, starting at 4.96 mg g^{-1} and reaching a peak of 21.40 mg g^{-1} at 80 mg L^{-1}, before slightly decreasing to 21.20 mg g^{-1} at 100 mg L^{-1} (Fig. 8b). This superior performance of PWSH@ZnO can be attributed to the enhanced surface area and additional adsorption sites provided by the incorporation of ZnO-NPs, which are known to significantly improve the adsorption characteristics of materials.

Despite the increase in adsorption capacity with rising NH_4^+ concentrations, both materials exhibit a notable decrease in removal efficiency. For PWSH, the removal efficiency drops from 77.25% at 10 mg L^{-1} to 36.76% at 100 mg L^{-1}, while PWSH@ZnO retains a higher removal efficiency, decreasing from 99.37% to 42.41% within the same concentration range. This inverse relationship between NH_4^+ concentration and removal efficiency is a typical phenomenon in adsorption processes, where increasing concentration leads to the saturation of available adsorption sites, thus limiting the amount of NH_4^+ that can be effectively removed.[73–75] Notably, despite the decline in removal efficiency, PWSH@ZnO consistently outperforms PWSH, highlighting its superior adsorption capacity and potential.

As NH_4^+ concentrations increase, both materials reach saturation, where adsorption capacity plateaus. Saturation occurs when all adsorption sites are occupied, preventing further adsorption despite increased NH_4^+ concentration. PWSH reaches saturation at ~18.38 mg g^{-1} (100 mg L^{-1}), while PWSH@ZnO achieves a higher capacity of 21.40 mg g^{-1} (80–100 mg L^{-1}). The higher capacity of PWSH@ZnO suggests that ZnO nanoparticles enhance surface area and active sites, facilitating greater NH_4^+ adsorption before saturation.[53,76] Once saturation is reached, additional NH_4^+ does not increase adsorption capacity, as all adsorption sites are occupied. This behavior highlights the adsorbent's efficiency limitations at high concentrations and underscores PWSH@ZnO's superior

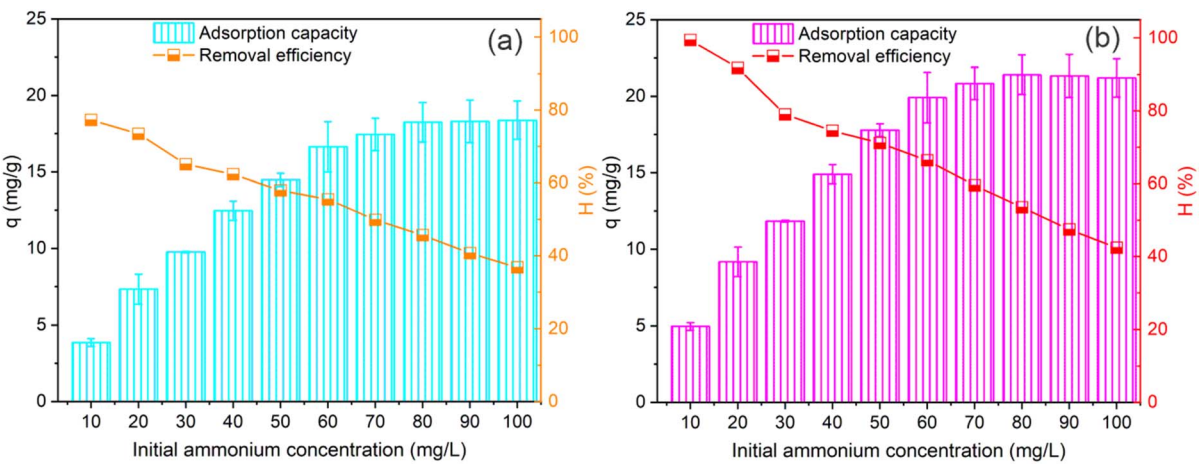

Fig. 8 Effect of NH_4^+ concentration on adsorption capacity and efficiency using PWSH (a) and PWSH@ZnO (b) materials, experimental conditions: contact time of 120 min; adsorbent dosage 2 g L^{-1}, pH 8.

performance in maintaining higher adsorption potential under elevated NH_4^+ concentrations. The findings show that both materials exhibit increasing adsorption capacity with rising NH_4^+ concentrations, eventually reaching saturation. The superior adsorption capacity and efficiency of PWSH@ZnO make it a promising candidate for wastewater treatment, where variable NH_4^+ concentrations require high-capacity, efficient adsorbents.[77–79]

Fig. 9 and Table 2 present the isotherm models for NH_4^+ adsorption onto PWSH and PWSH@ZnO, employing three commonly used models: Langmuir, Freundlich and Sips. These isotherms provide valuable insights into the interactions between NH_4^+ ions and the adsorbent materials, helping to characterize the nature of the adsorption process and assess the adsorption capacity of both materials.

The Langmuir model assumes monolayer adsorption on a homogeneous surface with a finite number of identical adsorption sites. For PWSH, the Langmuir model predicts a maximum adsorption capacity (Q_{max}) of 20.09 mg g^{-1}, with a Langmuir constant (K_L) of 0.2001 L mg^{-1}, indicating a moderate affinity between NH_4^+ ions and the adsorbent. The R^2 value of 0.9060 suggests that the Langmuir model provides a reasonable fit for the adsorption process on PWSH. In comparison, for PWSH@ZnO, the Langmuir model predicts a higher adsorption capacity of 23.08 mg g^{-1} and a K_L of 0.241 L mg^{-1}, implying a stronger interaction between NH_4^+ ions and the modified surface. The R^2 value of 0.8834 indicates that while the model fits the data well, it is slightly less accurate compared to the fit for PWSH.[80]

The Freundlich model, which assumes heterogeneous adsorption on a non-uniform surface with varying adsorption site energies, provides distinct results for both materials. For PWSH, the Freundlich constant (K_F) is 7.072 (mg g^{-1})/(mg L^{-1})^n, and the heterogeneity factor (n_F) is 3.918, indicating favorable adsorption with a strong affinity for NH_4^+ at low concentrations. The higher R^2 value of 0.9175 suggests that the Freundlich model better fits the PWSH adsorption data compared to the Langmuir model. In the case of PWSH@ZnO, the Freundlich model yields a higher K_F value of 9.008 and an n_F of 4.0, signifying a stronger adsorption affinity, especially at lower concentrations. However, the lower R^2 value of 0.7959 indicates that the Freundlich model does not fully capture the adsorption process for PWSH@ZnO, suggesting that it may not entirely reflect the complexity of the adsorption behavior on the ZnO-modified material.[81]

The Sips model, which combines aspects of the Langmuir and Freundlich models, is used to describe adsorption on heterogeneous surfaces. It accounts for both monolayer adsorption at low concentrations and multilayer adsorption at higher concentrations. For PWSH, the Sips model predicts Q_{max} of 20.62 mg g^{-1}, with a constant (b) of 0.343 and an n value of 1.0, reflecting balanced adsorption behavior. However, the low R^2 value of 0.6789 indicates that the Sips model is not the optimal fit for PWSH. In the case of PWSH@ZnO, the Sips

Table 2 Parameters and correlation coefficients of the NH_4^+ adsorption isotherm models using PWSH and PWSH@ZnO

Langmuir model			
	Q_{max}	K_L	R^2
Unit	mg g^{-1}	L mg^{-1}	
PWSH	20.09 ± 1.05	0.2001 ± 0.05	0.9060
PWSH@ZnO	23.08 ± 1.57	0.241 ± 0.08	0.8834
Freundlich model			
	K_F	n_F	R^2
Unit	(mg g^{-1})/(mg L^{-1})^n		
PWSH	7.072 ± 0.09	3.918 ± 0.07	0.9175
PWSH@ZnO	9.008 ± 0.12	4.0 ± 0.06	0.7959
Sips model			
	Q_{max}	b	n	R^2
Unit	mg g^{-1}			
PWSH	20.62 ± 0.28	0.343 ± 0.01	1.0 ± 0.03	0.6789
PWSH@ZnO	24.5 ± 0.31	0.336 ± 0.01	1.0 ± 0.04	0.6731

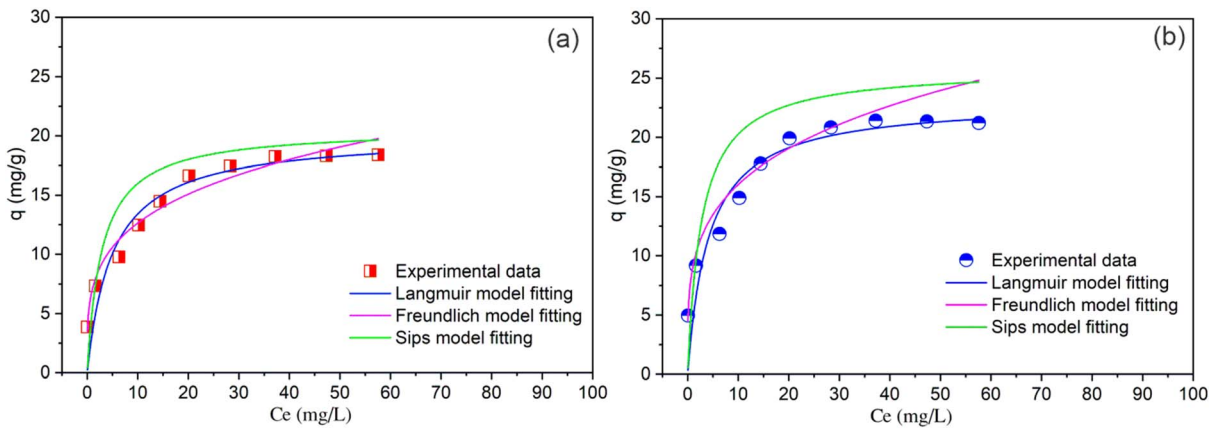

Fig. 9 Ammonium adsorption isotherm model using PWSH (a) and PWSH@ZnO (b).

model predicts a higher maximum adsorption capacity of 24.5 mg g^{-1}, with a b value of 0.336 and $n = 1.0$, suggesting similar adsorption characteristics to PWSH. However, the relatively low R^2 value of 0.6731 indicates that the Sips model does not fully capture the complexity of the adsorption process on the ZnO-modified material.[82]

In comparing the adsorption models, it is evident that both the Langmuir and Freundlich models provide a better fit for the experimental data than the Sips model, suggesting that the adsorption process is primarily dominated by monolayer adsorption on either homogeneous or heterogeneous surfaces. The higher Q_{max} values for PWSH@ZnO across all models reflect the enhanced adsorption capacity of the ZnO-modified material, likely due to its increased surface area and the additional active sites provided by the ZnO nanoparticles.[83] The Freundlich model's slightly better fit for PWSH suggests that adsorption on this material occurs on a more heterogeneous surface with varying adsorption site energies. In contrast, the Langmuir model offers a more accurate representation for PWSH@ZnO, indicating that the ZnO modification renders the surface more homogeneous, characterized by a finite number of high-energy adsorption sites.[84]

In summary, the Langmuir model provides the best fit for the adsorption isotherms of NH_4^+ on both PWSH and PWSH@ZnO, particularly for the latter, suggesting monolayer adsorption on a relatively homogeneous surface. The higher adsorption capacity of PWSH@ZnO indicates that the incorporation of ZnO nanoparticles significantly enhances the material's ability to adsorb NH_4^+, making it a more effective adsorbent for practical applications in NH_4^+ removal. The Freundlich model fits the adsorption data for PWSH, indicating heterogeneous adsorption, while the Sips model provides a less accurate description for both materials.

Ammonium adsorption mechanism and PWSH@ZnO recyclability

The adsorption mechanisms of NH_4^+ onto PWSH and PWSH@ZnO are governed by a combination of physical and chemical processes. PWSH@ZnO exhibits significantly enhanced performance due to the synergistic effects of the ZnO nanoparticles. The primary mechanisms responsible for this enhanced adsorption include electrostatic attraction, cation exchange, surface complexation, physical adsorption, and cation–π interactions. These mechanisms collectively optimize the capture of NH_4^+ ions from aqueous solutions (Fig. 10). They contribute to the materials' overall adsorption capacity and efficiency, especially at an optimal pH of 8, where surface charge interactions and chemical affinity are most favorable.[85,86]

Electrostatic attraction plays a pivotal role in the adsorption of NH_4^+ ions, particularly when considering the solution's pH, the point of zero charge (pH_{PZC}) and the zeta potential of the adsorbent. The zeta potential of PWSH is measured at −7.3 mV, indicating a negative surface charge. This negative charge leads to electrostatic repulsion between the surface of PWSH and negatively charged ions, while simultaneously attracting positively charged NH_4^+ ions. In contrast, the zeta potential of PWSH@ZnO is +6.5 mV, signifying a positive surface charge that favors electrostatic attraction between the PWSH@ZnO surface and NH_4^+ ions, thus enhancing adsorption efficiency. This favorable electrostatic interaction, particularly at pH 8,

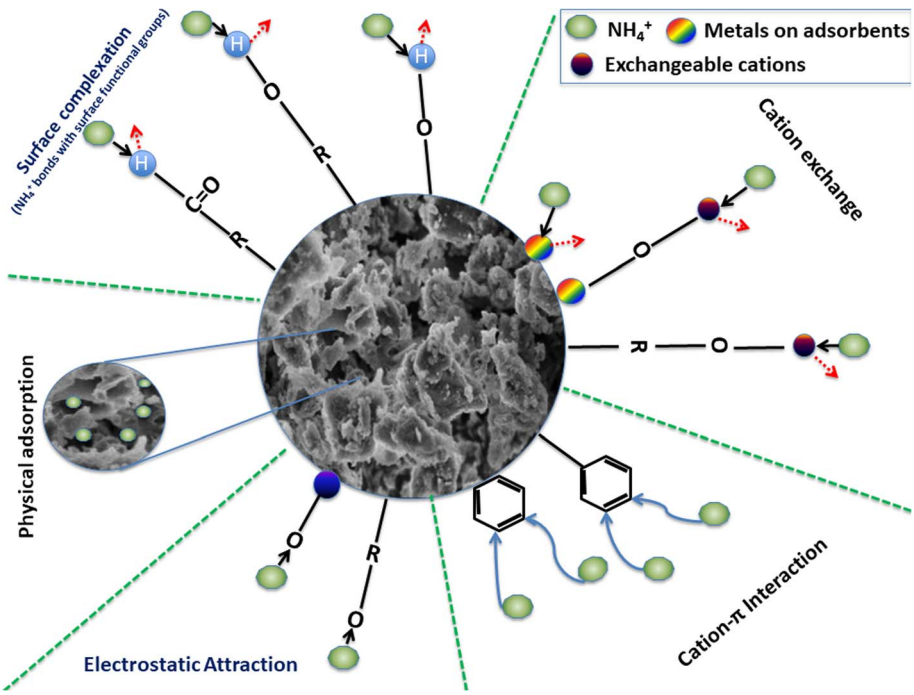

Fig. 10 Ammonium adsorption onto PWSH and PWSH@ZnO.

combined with the stability of NH_4^+ in solution, results in improved adsorption capacity. Furthermore, the pH_{PZC} of PWSH is approximately 7.8, suggesting that at pH levels above this threshold, the material's surface acquires a negative charge. This negative charge enhances electrostatic attraction with the positively charged NH_4^+ ions. At pH 8, which is slightly above the pH_{PZC}, the surface charge of PWSH is predominantly negative, creating a favorable environment for NH_4^+ adsorption. However, since the pH is close to the pH_{PZC}, the electrostatic attraction may not be as pronounced as it would be at higher pH levels. This could lead to a moderate decrease in adsorption efficiency compared to conditions where the pH is significantly above the pH_{PZC}. Despite this, PWSH still demonstrates considerable adsorption capacity, primarily due to its inherent surface chemistry and structural characteristics. The presence of functional groups on the surface of PWSH enables alternative adsorption mechanisms, such as cation exchange and physical adsorption, which further contribute to the removal of NH_4^+ ions, even when electrostatic forces are less dominant.[87]

In contrast, PWSH modified with ZnO (PWSH@ZnO) exhibits enhanced adsorption performance due to the synergistic effects of the ZnO nanoparticles. The pH_{PZC} of PWSH@ZnO is approximately 8.3, indicating that at pH 8, the surface remains negatively charged, thereby maintaining a favorable electrostatic environment for NH_4^+ adsorption. The ZnO-NPs increase the surface area and introduce additional reactive sites that can participate in cation exchange and surface complexation processes. These mechanisms can effectively compensate for any reduction in electrostatic attraction, allowing PWSH@ZnO to achieve higher NH_4^+ adsorption efficiency than PWSH alone. The diminished role of electrostatic attraction in both materials at pH 8 can be attributed to their proximity to their respective pH_{PZC} values, where the surface charge is minimal. Nonetheless, the enhanced surface properties of PWSH@ZnO enable it to outperform PWSH in NH_4^+ adsorption due to the combined effects of electrostatic attraction, cation exchange, and surface complexation.[88,89]

Cation exchange is a critical mechanism for the adsorption of NH_4^+ in both PWSH and PWSH@ZnO. This process involves the exchange of NH_4^+ ions in solution with cations (*e.g.*, H^+, Na^+ or Ca^{2+}) from the surface of the adsorbent. Both materials possess oxygenated functional groups, such as hydroxyl (–OH) and carboxyl (–COOH), which facilitate this exchange process. In PWSH@ZnO, the incorporation of ZnO nanoparticles increases the number of reactive sites on the surface, thereby enhancing the overall cation exchange capacity of the material. The general reaction for cation exchange in both materials can be expressed as (7):

$$R–OH + NH_4^+ \leftrightarrow R–NH_4^+ + H^+ \quad (7)$$

In this reaction, R–OH represents the hydroxyl groups present on the surface of the adsorbent, which exchange with NH_4^+ ions from the solution. This cation exchange mechanism is particularly effective at pH 8, where NH_4^+ is the predominant species in the solution. The incorporation of ZnO nanoparticles in PWSH@ZnO significantly enhances the material's surface area and porosity, thereby facilitating a more efficient exchange process and resulting in a higher adsorption capacity compared to unmodified PWSH. Although cation exchange also occurs in PWSH, its effectiveness is limited due to the lower surface area and fewer functional groups available for exchange.[90,91]

Surface complexation is another critical mechanism that enhances NH_4^+ adsorption, particularly in PWSH@ZnO. This process involves the formation of chemical bonds between NH_4^+ ions and functional groups on the adsorbent's surface. The incorporation of ZnO nanoparticles into the hydrochar increases the number of available surface sites for complexation, thereby improving the material's overall adsorption capacity. The surface complexation reaction can be expressed as (8):

$$R–C{=}O + NH^+ \leftrightarrow R–C{=}O - NH_4^+ \quad (8)$$

In this process, R–COOH represents the carboxyl groups on the adsorbent's surface, which form stable complexes with NH_4^+ ions. This mechanism plays a pivotal role in PWSH@ZnO, where the incorporation of ZnO nanoparticles significantly enhances surface reactivity, facilitating stronger chemical bonds between NH_4^+ and the adsorbent. These bonds are more stable than those formed *via* physical adsorption, thereby contributing to a higher overall adsorption capacity. In contrast, PWSH also undergoes surface complexation, though it is less efficient due to the absence of ZnO-NPs, leading to a greater reliance on weaker adsorption mechanisms, such as physical adsorption and cation exchange.[92,93]

Physical adsorption, primarily through pore filling, is another critical mechanism for NH_4^+ removal in both PWSH and PWSH@ZnO. The incorporation of ZnO nanoparticles significantly enhances the surface area and porosity, thereby improving the material's NH_4^+ adsorption efficiency. This type of adsorption is governed by van der Waals forces, which, although weaker than chemical bonding, still play a notable role in the overall adsorption capacity of the material. BET surface area analysis shows that PWSH@ZnO exhibits a significantly higher surface area than unmodified PWSH, contributing to its enhanced porosity. This increase in surface area provides additional sites for physical adsorption, facilitating greater NH_4^+ uptake. The pore-filling mechanism is confirmed by a reduction in pore volume and surface area after NH_4^+ adsorption, suggesting that the NH_4^+ ions occupy the available pores on the adsorbent surface. In contrast, PWSH, with its lower surface area and fewer pores, relies more on chemical interactions, such as cation exchange and surface complexation, rather than physical adsorption. This limitation in surface area restricts the material's overall adsorption capacity, making PWSH@ZnO more efficient for NH_4^+ removal.[94,95]

A more subtle but important mechanism in the adsorption process for PWSH is the cation–π interaction. The carbon-rich structure of hydrochar, derived from paper waste sludge, contains aromatic rings with delocalized π-electrons. These π-electrons can interact with the positively charged NH_4^+ ions, forming cation–π interactions that contribute to the overall adsorption process. This interaction is particularly significant

in PWSH, as the absence of ZnO nanoparticles limits the material's reliance on other adsorption mechanisms. In contrast, cation–π interactions are less prominent in PWSH@ZnO, where mechanisms such as surface complexation and cation exchange dominate. However, in PWSH, this mechanism plays a more crucial role in compensating for the lower surface area and fewer functional groups available for chemical adsorption.[57,96]

Therefore, NH_4^+ adsorption onto PWSH and PWSH@ZnO involves a combination of electrostatic attraction, cation exchange, surface complexation, physical adsorption, and cation-π interactions. PWSH@ZnO exhibits superior adsorption performance due to the presence of ZnO nanoparticles, which increase the surface area, introduce additional functional groups, and strengthen electrostatic interactions and surface complexation. These synergistic effects make PWSH@ZnO a highly effective adsorbent for NH_4^+ removal, particularly in wastewater treatment applications. In contrast, while PWSH remains effective, it relies more heavily on weaker adsorption mechanisms, resulting in a lower adsorption capacity compared to its ZnO-modified counterpart.

The recyclability of PWSH@ZnO for NH_4^+ adsorption was evaluated over five cycles, as shown in Fig. 11. The initial adsorption capacity (q) was 21.33 mg g^{-1} in the first cycle. In the second cycle, the adsorption capacity decreased slightly to 20.42 mg g^{-1}. With each subsequent cycle, the adsorption capacity continued to decline. By the fifth cycle, the adsorption capacity decreased to 12.68 mg g^{-1}, indicating a significant reduction in efficiency. This trend suggests that PWSH@ZnO's performance declines with repeated use, likely due to the partial loss of active sites during desorption and reuse. While effective in the initial cycles, the adsorbent's efficiency gradually decreases. This reduction may result from exhausted adsorption sites, structural changes, or blocked active sites due to residual contaminants. The significant drop in adsorption capacity by the fifth cycle suggests limited durability for long-term reuse without regeneration or modification to improve stability and capacity retention. Therefore, strategies like periodic regeneration or structural modifications may be needed to enhance PWSH@ZnO's longevity and performance for practical applications.

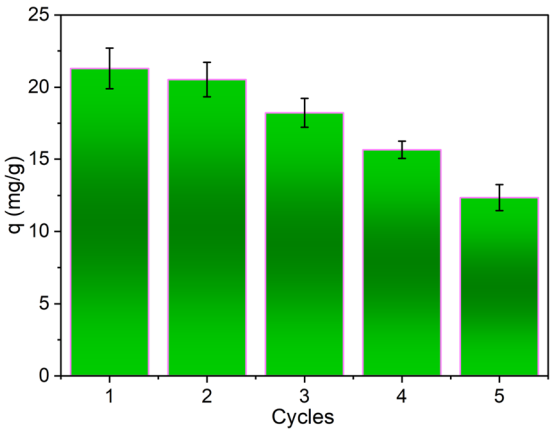

Fig. 11 The recyclability of the PWSH@ZnO for NH_4^+ adsorption.

Conclusion

The research demonstrated that the modification of paper waste sludge hydrochar (PWSH) with ZnO nanoparticles (ZnO-NPs) significantly enhances its capacity and efficiency for NH_4^+ adsorption. The ZnO-NP-modified hydrochar (PWSH@ZnO) exhibited a superior adsorption capacity of 23.08 mg g^{-1}, compared to 20.09 mg g^{-1} for the unmodified PWSH. The solution pH played a crucial role in the adsorption process, with optimal performance occurring at pH 8, where PWSH@ZnO achieved a remarkable removal efficiency of 80%. Kinetic analysis indicated that both materials adhered to the pseudo-first-order model, with PWSH@ZnO exhibiting faster adsorption rates, which suggests that the ZnO modification enhanced the material's reactivity and surface characteristics. Isotherm modelling, primarily using the Langmuir model, further supported the conclusion that NH_4^+ adsorption on PWSH@ZnO follows a monolayer adsorption process on a homogeneous surface. These findings highlight the potential of PWSH@ZnO as a cost-effective and environmentally sustainable adsorbent for NH_4^+ removal from wastewater, indicating its applicability in large-scale treatment systems. Moreover, the PWSH@ZnO composites demonstrated efficient ammonium adsorption performance and commendable recyclability, maintaining a significant portion of their adsorption capacity over five consecutive adsorption–desorption cycles.

Although the results obtained from the application of PWSH@ZnO are promising, several practical challenges need to be addressed to enable its real-world implementation. Key issues include improving the regeneration of the adsorbent for sustained long-term performance, ensuring the stability of zinc oxide nanoparticles (ZnO-NPs) under varying environmental conditions, and evaluating the cost-effectiveness of large-scale production and application. Future research should prioritize optimizing regeneration processes, developing cost-efficient synthesis methods, and assessing the adsorbent's performance in real wastewater systems, which are often characterized by complex matrices. Furthermore, advanced characterization techniques could provide valuable insights into the mechanisms underlying NH_4^+ adsorption. Additionally, investigating the environmental implications of disposing of spent adsorbents and exploring their potential for reuse, such as in soil amendment, could significantly enhance the sustainability of this approach. Addressing these challenges and pursuing these research directions will contribute to advancing PWSH@ZnO as a scalable and sustainable solution for ammonium removal in wastewater treatment processes.

Data availability

Data associated with this study has not been deposited into a publicly available repository. Data will be made available on request.

Author contributions

Trung Kien Hoang, Thi Dong Nguyen: conceived and planned the experiments; Thi Hong Vien Nguyen: collected, prepared

ZnO nanoparticles composited fly ash; Thi Hong uyen Chu carried out experiments; Le Phuong Hoang, Thi Minh Phuong Nguyen: contributed to analysis samples before and after experimental processes; Van Hung Hoang contributed to the interpretation of the results; Phan Quang Thang, Le Phuong Hoang, Lan Huong Nguyen and Huu Tap Van wrote the manuscript.

Conflicts of interest

The authors have not disclosed any competing interests.

Acknowledgements

This work was financially supported by Vietnam Ministry of Education and Training under project number: B2024-TNA-07.

References

1 L. H. Nguyen, H. T. Van, Q. T. Nguyen, T. H. Nguyen, T. B. L. Nguyen, V. Q. Nguyen, T. U. Bui and H. Le Sy, *J. Water Process. Eng.*, 2021, **39**, e101877.
2 Z. Hu, T. Lotti, M. C. M. van Loosdrecht and B. Kartal, *Biotechnol. Lett.*, 2013, **35**, 1145–1154.
3 Y. Zhao, B. Zhang, Z. Xiang, J. Wang, J. Liu and R. Chen, *Water Sci. Technol.*, 2010, **62**, 937–946.
4 M. Rodrigues, T. T. de Mattos, T. Sleutels, A. ter Heijne, H. V. M. Hamelers, C. J. N. Buisman and P. Kuntke, *ACS Sustainable Chem. Eng.*, 2020, **8**, 17359–17367.
5 S. Hube, M. Eskafi, K. F. Hrafnkelsdóttir, B. Bjarnadóttir, M. Á. Bjarnadóttir, S. Axelsdóttir and B. Wu, *Sci. Total Environ.*, 2020, **710**, e136375.
6 X. Wang, M. Sun, Y. Zhao, C. Wang, W. Ma, M. S. Wong and M. Elimelech, *Environ. Sci. Technol.*, 2020, **54**, 6997–7007.
7 E. Ivanova, M. Karsheva and B. Koumanova, *J. Univ. Chem. Technol. Metall.*, 2010, **45**, 295–302.
8 F. Al-Sheikh, C. Moralejo, M. Pritzker, W. A. Anderson and A. Elkamel, *Sep. Sci. Technol.*, 2021, **56**, 462–473.
9 J. Kim, H. Lee, H. Thanh Vo, G. Lee, N. Kim, S. Jang and J. B. Joo, *Materials*, 2020, **13**, e1375.
10 Q. Yu, D. Xia, H. Li, L. Ke, Y. Wang, H. Wang, Y. Zheng and Q. Li, *RSC Adv.*, 2016, **6**, 88373–88381.
11 R. B. Fidel, D. A. Laird and K. A. Spokas, *Sci. Rep.*, 2018, **8**, 1–10.
12 Y. Huang and W. Shama, *New J. Chem.*, 2024, **48**, 10019–10025.
13 H. R. Sobhi, M. Yeganeh, M. Ghambarian, S. Fallah and A. Esrafili, *RSC Adv.*, 2024, **14**, 16617–16623.
14 W. C. Qian, X. P. Luo, X. Wang, M. Guo and B. Li, *Ecotoxicol. Environ. Saf.*, 2018, **157**, 300–306.
15 X. Zhang, Y. Wang, J. Cai, K. Wilson and A. F. Lee, *Energy Environ. Mater.*, 2020, **3**, 1–16.
16 N. Chai, L. Gao, S. Li, Z. Ma, L. Li and M. Hu, *Sustainability*, 2023, **15**, e11867.
17 S. Oumabady, S. P. Ramasamy, S. P. Sebastian, R. Rajagopal, P. K. Obulisamy, R. Doherty, S. Nanukuttan, S. D. Bhardwaj and D. Kumaresan, *J. Sustainable Agric. Environ.*, 2023, **2**, 328–336.
18 R. Isemin, N. S. Muratova, S. Kuzmin, Д. В. Климов, В. С. Коч-Татаренко, A. V Mikhalëv, O. Y. Milovanov, A. Dalibard, O. A. Ibitowa, M. Nowotny, M. Brulé, F. Tabet and B. Rogge, *Processes*, 2021, **9**, e2082.
19 H. A. Al-Swadi, A. S. Al-Farraj, M. I. Al-Wabel, M. Ahmad, J. Ahmad, M. A. Mousa, M. I. Rafique and M. Usama, *Sustainability*, 2023, **15**, e15978.
20 Mankomal and H. Kaur, *Appl. Surf. Sci. Adv.*, 2022, **12**, e100339.
21 J. Yu, C. Jiang, Q. Guan, P. Ning, J. Gu, Q. Chen, J. Zhang and R. Miao, *Chemosphere*, 2018, **195**, 632–640.
22 M. C. Monte, E. Fuente, A. Blanco and C. Negro, *J. Waste Manage.*, 2009, **29**, 293–308.
23 A. Yaras and H. Arslanoğlu, *Arabian J. Sci. Eng.*, 2018, **43**, 2393–2402.
24 K. Nalwa, *Adv. Mater. Processes*, 2021, **2**, 697–703.
25 T. D. Pham, T.-T.-T. Truong, H.-L. Nguyen, L.-B.-L. Hoang, V.-P. Bui, T.-T.-M. Tran, T. B. H. Dinh and T. A. Le, *ACS Omega*, 2022, **7**, 42073–42082.
26 C. X. Hu, *Mater. Sci. Forum*, 2022, **1058**, 33–38.
27 S. Aftab, T. Shabir, A. Shah, J. Nisar, I. Shah, H. Muhammad and N. S. Shah, *Nanomaterials*, 2022, **12**, e486.
28 A. T. Le, S.-Y. Pung, S. Sreekantan, A. Matsuda and D. P. Huynh, *Heliyon*, 2019, **5**, e01440.
29 A. Zhao, Q. Tang, Y. Chen, C. Qiu and X. Huang, *Molecules*, 2023, **28**, e6499.
30 M. Krasovska, V. Gerbreders, E. Tamanis, S. Gerbreders and A. Bulanovs, *Latv. J. Phys. Tech. Sci.*, 2017, **54**, 41–50.
31 F. B. Kheyrabadi and E. N. Zare, *Sci. Rep.*, 2022, **12**, e4632.
32 D. Chen, W. Shen, S. Wu, C. Chen, X. Luo and L. Guo, *Nanoscale*, 2016, **8**, 7172–7179.
33 X. Zhu, Y. Liu, F. Qian, Z. Lei, Z. Zhang, S. Zhang, J. Chen and Z. J. Ren, *Environ. Sci. Technol.*, 2017, **51**, 10756–10764.
34 G. Tondl, C. Hammerl, C. Pfeifer and D. Pum, *Ind. Eng. Chem. Res.*, 2020, **59**, 1829–1835.
35 H. H. Farghal, M. Nebsen and M. M. H. El-Sayed, *RSC Adv.*, 2023, **13**, 19757–19769.
36 X. Chen, B. Li, Y. Shen and J.-Z. Guo, *ACS Omega*, 2019, **4**, 15022–15029.
37 A. Khataee, B. Kayan, D. Kalderis, A. Karimi, S. Akay and M. Konsolakis, *Ultrason. Sonochem.*, 2017, **35**, 72–80.
38 A. Kruse, F. Koch, K. Stelzl, D. Wüst and M. Zeller, *Energy Fuels*, 2016, **30**, 8037–8042.
39 X. Cao, K. S. Ro, J. A. Libra, C. Kammann, I. M. Lima, N. D. Berge, L. Li, Y. Li, N. Chen, J. Yang, B. Deng and J. Mao, *J. Agric. Food Chem.*, 2013, **61**, 9401–9411.
40 M. Hessien, *Molecules*, 2023, **28**, e4526.
41 S. Ekinci, *J. Chin. Chem. Soc.*, 2023, **71**, 84–98.
42 Z. Hu, X. Chen and H. Jiang, *ACS ES&T Eng.*, 2022, **3**, 165–173.
43 X. Zhu, Y. Liu, F. Qian, C. Zhou, S. Zhang and J. Chen, *ACS Sustainable Chem. Eng.*, 2015, **3**, 833–840.
44 V. Mau, G. Arye and A. Gross, *PLoS One*, 2018, **13**, e0206299.
45 H. Lin, Y. Jiang, Z. Yi, L. Zhang, S. Zhang, K. Ding, B. Li, S. Wang and X. Hu, *ACS Food Sci. Technol.*, 2023, **3**, 1098–1110.

46 L. Zhang, J. Tan, G. Xing, X. Dou and X. Guo, *Bioresour. Bioprocess.*, 2021, **8**, e10.
47 P. T. Tho, H. T. Van, L. H. Nguyen, T. K. Hoang, T. N. Ha Tran, T. T. Nguyen, T. B. Hanh Nguyen, V. Q. Nguyen, H. Le Sy, V. N. Thai, Q. B. Tran, S. M. Sadeghzadeh, R. Asadpour and P. Q. Thang, *RSC Adv.*, 2021, **11**, 18881–18897.
48 J. Abdulsalam, K. O. Otun, N. Gardee, B. Patel, T. Y. Leswifi and M. K. Mathe, *ACS Omega*, 2023, **8**, 5285–5299.
49 L. Han, K. S. Ro, K. Sun, H. Sun, Z. Wang, J. A. Libra and B. Xing, *Environ. Sci. Technol.*, 2016, **50**, 13274–13282.
50 J. S. J. Bharti, G. Kumar, V. Kumar and A. Kumar, *SN Appl. Sci.*, 2021, **3**, e311.
51 Z. Mirzaeifard, Z. Shariatinia, M. Jourshabani and S. M. R. Darvishi, *Ind. Eng. Chem. Res.*, 2020, **59**, 15894–15911.
52 M. N. Pour, H. A. Rangkooy, F. Jahani, A. Golbaghi, H. S. F. Abady and L. Nematpour, *Environ. Health Eng. Manage. J.*, 2019, **6**, 225–232.
53 H. Huang, X. Xiao, B. Yan and L. Yang, *J. Hazard. Mater.*, 2010, **175**, 247–252.
54 F. Pantoja, S. Beszédes, T. Gyulavári, E. Illés, G. Kozma and Z. László, *Heliyon*, 2024, **10**, e31495.
55 C. Zhang, H. Wang, Q. Chang and J. Zhang, in *7th International Conference on Energy and Environmental Protection*, 2018, pp. 1470–1475.
56 J. Wang, T. Tsuzuki, B. Tang, X. Hou, L. Sun and X. Wang, *ACS Appl. Mater. Interfaces*, 2012, **4**, 3084–3090.
57 L. Lin, Z. Lei, L. Wang, X. Liu, Y. Zhang, C. Wan, D. J. Lee and J. H. Tay, *Sep. Purif. Technol.*, 2013, **103**, 15–20.
58 E. Leiva, C. Tapia and C. Rodríguez, *Molecules*, 2021, **26**, e2713.
59 R. Al-Saedi, Z. A. Hammood and T. F. Chyad, *J. Ecol. Eng.*, 2021, **22**, 188–194.
60 K. R. Raghupathi, R. T. Koodali and A. La Manna, *Langmuir*, 2011, **27**, 4020–4028.
61 Z. You, C. Zhuang, Y. Sun, S. Zhang and H. Zheng, *Ind. Eng. Chem. Res.*, 2019, **58**, 14528–14537.
62 M. Alam, N. M. Alandis, A. A. Ansari and M. R. Shaik, *J. Nanomater.*, 2013, **14**, e2106.
63 J. Xue, S. Ma, Y. Zhou, Z. Zhang and P. Jiang, *RSC Adv.*, 2015, **5**, 18832–18840.
64 C. Karunakaran, P. Vinayagamoorthy and J. Jayabharathi, *Langmuir*, 2014, **30**, 15031–15039.
65 H. Hsi, C.-T. Tsai and K.-J. Lin, *Energy Fuels*, 2014, **28**, 3300–3309.
66 L. Ji and Y. J. Yuan, *Langmuir*, 2014, **30**, 9637–9642.
67 P. Kumar, M. Govindaraju and V. Sivakumar, *Anti-Corros. Methods Mater.*, 2018, **65**, 19–33.
68 Y. Fan, Q. Weng, Y. Zhuo, S. Dong, P. Hu and D. Li, *Materials*, 2019, **12**, e677.
69 Y. Zhang, W. Shi, H. Zhou, X. Q. Fu and X. Chen, *Water Environ. Res.*, 2010, **82**, 567–573.
70 M. N. Idris, A. R. Daud and N. K. Othman, *Mater. Sci. Forum*, 2017, **888**, 382–388.
71 L. C. Murulana, A. K. Singh, S. K. Shukla, M. M. Kabanda and E. E. Ebenso, *Ind. Eng. Chem. Res.*, 2012, **51**, 13282–13299.
72 J. Ambrosy, C. Pasel, M. Luckas, M. Bittig and D. Bathen, *Chem. Ing. Tech.*, 2019, **91**, 1874–1884.
73 M. Zhang, G. Song, D. L. Gelardi, L. Huang, E. Khan, G. Xu, S. J. Parikh and K.-H. Kim, *Water Res.*, 2020, **186**, e116303.
74 H. Shen, C. Zhou, S. Xu, Y. Huang, J. Shi and G. Liu, *Water Environ. Res.*, 2023, **95**, e10905.
75 A. Khalil, N. Sergeevich and V. Borisova, *Adsorpt. Sci. Technol.*, 2018, **36**, 1294–1309.
76 G. Galamini, G. Ferretti, V. Medoro, N. Tescaro, B. Faccini and M. Coltorti, *Ecol. Footprints Hum. Act.*, 2020, **119**, e42.
77 B. Faccini, D. Di Giuseppe, G. Ferretti, M. Coltorti, N. Colombani and M. Mastrocicco, *Nutr. Cycling Agroecosyst.*, 2018, **110**, 327–341.
78 T. Çalban, B. Kaynarca, F. Sevim and H. Eroğlu, *Asian J. Chem.*, 2014, **26**, 6111–6117.
79 F. Xiao, X. Cao, X. Lyu, L. Li, J. Qiu, Y. Zhang, P. Wang, Q. Zhang and Q. Wang, *Environ. Prog. Sustainable Energy*, 2019, **39**, e13358.
80 S. Lan, L. Liu, R. Li, Z. Leng and S. Gan, *Ind. Eng. Chem. Res.*, 2014, **53**, 3131–3139.
81 S. Mahdavi, P. Molodi and M. Zarabi, *Environ. Prog. Sustainable Energy*, 2018, **37**, 1908–1917.
82 L. Lian, J. Lv and D. Lou, *ACS Sustainable Chem. Eng.*, 2017, **5**, 10298–10306.
83 R. Ragadhita and A. B. D. Nandiyanto, *Indones. J. Sci. Technol.*, 2021, **6**, 205–234.
84 K. G. Akpomie, S. Ghosh, M. Gryzenhout and J. Conradie, *Sci. Rep.*, 2021, **11**, 8305.
85 X. Li, L. Li, B. Qiao, X. Yang, A. Wang and X. Wang, *J. Phys. Chem. C*, 2018, **122**, 12395–12403.
86 H. Sadegh, G. A. M. Ali, Z. Abbasi and M. N. Nadagouda, *Stud. Univ. Babes-Bolyai, Chem.*, 2017, **62**, 233–245.
87 K. Mondal, M. Megha, A. Banerjee, A. Fortunelli, M. Walter and M. Moseler, *J. Phys. Chem. C*, 2021, **126**, 764–771.
88 M. Ali, N. Tit and Z. H. Yamani, *Int. J. Energy Res.*, 2020, **44**, 10926–10936.
89 E. Y. Shaba, J. O. Tijani, J. Jacob and M. Suleiman, *J. Chem. Technol. Biotechnol.*, 2022, **97**, 2196–2217.
90 T. He, H. Liu, J. Zhang, Y. Yang, Y. Jiang, Y. Zhang, J. Feng and K. Hu, *Nanomaterials*, 2023, **13**, e2510.
91 V. Sabadash, Я. М. Гумницький, O. Lyuta and I. Pochapska, *Chem. Chem. Technol.*, 2018, **12**, 143–146.
92 F. Peng, P. He, Y. Luo, X. Lu, Y. Liang and J. Fu, *Clean:Soil, Air, Water*, 2012, **40**, 493–498.
93 D. T. Nguyen, T. K. Phung, D. N. Vo, T. H. Le, Đ. Q. Khiếu and T. L. M. Pham, *RSC Adv.*, 2020, **10**, 40663–40672.
94 Y. Jing, Y. Lai, S. Zhang, R. Wang, Z. Xu and Y. Pei, *Crystals*, 2021, **12**, e34.
95 M. D. Nivison, D. L. Vandell, C. Booth-LaForce and G. I. Roisman, *Psychol. Sci.*, 2021, **32**, 721–734.
96 H. Liu, Z. Zheng, D. Yang, E. R. Waclawik, X. Ke, H. Zhu, S. J. Palmer and R. L. Frost, *J. Raman Spectrosc.*, 2010, **41**, 1601–1605.